1. Manuscript Title (50 word maximum) - Impaired reliability and precision of spiking in adults but not juveniles in a mouse model of Fragile X Syndrome

2. Abbreviated Title (50 character maximum) – Impaired spike reliability in Fragile X Syndrome.

3. List all Author Names and Affiliations in order as they would appear in the published article

Deepanjali Dwivedi [1], Sumantra Chattarji [1, 2, 3], Upinder S. Bhalla [1, 2]

[1] National Centre for Biological Sciences, TIFR, GKVK campus, Bellary Road, Bangalore 560065, India

[2] Centre for Brain Development and Repair, Institute for Stem Cell Biology and Regenerative Medicine, Bangalore 560065, India.

[3] Centre for Discovery Brain Sciences, Deanery of Biomedical Sciences, University of Edinburgh, Hugh Robson Building, 15 George Square, Edinburgh EH89XD, UK

4. Author Contributions: DD and USB designed the project. SC and USB provided the animals and equipments for the project. DD did the experiments and the analysis. DD and USB wrote the paper.

5. **Correspondence should be addressed to (include email address)**

Dr. Upinder S. Bhalla,

National Centre for Biological Sciences, TIFR, GKVK campus, Bellary Road, Bangalore.

E Mail ID – bhalla@ncbs.res.in

6. Number of Figures - 10

7. Number of Tables - 1

8. Number of Multimedia - 0

9. Number of words for Abstract - 237

10. Number of words for Significance Statement - 118

11. Number of words for Introduction - 660

12. Number of words for Discussion - 2301

13. Acknowledgements

I would like to thank Suranjana Pal, Bishal Basak, Vidya Ramesh, Sarfaraz Nawaz for help with Immunofluorescence experiments. I would also thank Giselle Fernandes, Shreya Das Sharma, Aviral Goel, Sathyaa Subramaniyam, Aanchal Bhatia and Sahil Moza for useful inputs from time to time.

14. Conflict of Interest

The Authors declare no competing financial interests.

15. Funding - DD was funded by NCBS/TIFR Intramural funds during the project. National Mouse Resource (NaMoR) and Department of Biotechnology (DBT) provided funds for mouse maintenance and experimental equipments.

Impaired reliability and precision of spiking in adults but not juveniles in a mouse model of Fragile X Syndrome

Abstract

Fragile X Syndrome (FXS) is the most common source of intellectual disability and autism. Extensive studies have been performed on the network and behavioral correlates of the syndrome but our knowledge about intrinsic conductance changes is still limited. In this study we show a differential effect of FMRP Knock Out (KO) in different sub-sections of hippocampus using whole cell patch clamp in mouse hippocampal slices. We observed no significant change in spike numbers in the CA1 region of hippocampus but a significant increase in CA3, in juvenile mice. However, in adult mice we see a reduction in spike number in the CA1 with no significant difference in CA3. In addition, we see increased variability in spike number in CA1 cells following a variety of steady and modulated current step protocols. This effect emerges in adult (8 weeks) but not juvenile (4 weeks) mice. This increased spiking variability was correlated with reduced spike number and with elevated AHP. The increased AHP arose from elevated SK currents (small conductance calcium activated potassium channels) but other currents involved in mAHP, such as I_h and M, were not significantly different. We obtained a partial rescue of the cellular variability phenotype when we blocked SK current using the specific blocker apamin. Our observations provide a single cell correlate of the network observations of response variability and loss of synchronization, and suggest that elevation of SK currents in FXS may provide a partial mechanistic explanation for this difference.

Significance Statement

Fragile-X syndrome leads to a range of intellectual disability effects and autism. We have found differential effect of FMRP KO in different sub sections of hippocampus where it caused an increased spiking in CA3 in juveniles and reduced spiking in CA1, in adults. We have also found that even individual neurons with this mutation exhibit increased variability in their activity patterns. Importantly, this effect emerges after six weeks of age in mice. We showed that a specific ion channel protein, SK channel, was partially responsible, and blockage of these channels led to a partial restoration of cellular activity. This is interesting as it provides a possible molecular link between activity variability in single cells, and reported irregularity in network activity.

103

104 **INTRODUCTION**

105 Fragile X Syndrome (FXS) is an autism spectrum disorder arising from increased
106 repeats of CGG tri-nucleotide in the FMR1 gene. This leads to silencing of the gene
107 and hence the absence of the FMRP protein. (O'Donnell and Warren, 2002). FMRP
108 is a transcription factor which affects multiple downstream genes including ion
109 channels (Brown et al., 2001; Darnell et al., 2011). Studies have shown that
110 absence of FMRP affects the functioning of ion channels either by regulating the
111 number of channels (Meredith et al., 2007; Strumbos et al., 2010; Gross et al., 2011;
112 Lee et al., 2011; Routh et al., 2013; Ferron et al., 2014; Zhu et al., 2018) or by
113 directly interacting with the channels (Brown et al., 2010; Deng et al., 2013). Multiple
114 studies have shown that potassium channels have a significant effect on spike
115 precision (Fricker and Miles, 2000; Gittelman, 2006; Cudmore et al., 2010), and
116 many of these potassium channels are transcription hits for FMRP. This leads to the
117 hypothesis that FXS may alter the functioning of one or multiple potassium channels,
118 leading to effects on spike precision.

119 In recent years a number of in-vivo hippocampal recording studies have
120 shown that there is poor correlation of spiking activity between cells, and abnormal
121 theta-gamma phase coupling in FXS mice (Radwan et al., 2016; Arbab et al., 2018;
122 Talbot et al., 2018). In medial Prefrontal Cortex (mPFC), variability in calcium (Ca^{2+})
123 responses has also been observed, leading to impaired Spike Timing Dependent
124 Plasticity (STDP) (Meredith et al., 2007).These studies have led to the
125 'discoordination hypothesis' for FXS (Talbot et al., 2018). This hypothesis states that
126 neurons in FXS are uncorrelated and have aberrant network discharges. In apparent
127 contradiction to this hypothesis, neurons showed hyper connectivity and

synchronization in cortical networks of FXS model mice (Testa-Silva et al., 2012; Gonçalves et al., 2013)

Synchronicity is an emergent property of a network and is a function of both network connectivity and intrinsic properties. Specifically, potassium conductances have been shown to have significant effects on spike precision and network synchrony (Fricker and Miles, 2000; Pfeuty et al., 2003; Deister et al., 2009; Cudmore et al., 2010; Gastrein et al., 2011; Hou et al., 2012). Modeling studies have also shown that conductances which mediate spike frequency adaptation help to synchronize network firing (Crook et al., 1998). I_h currents, I_M currents and SK currents have been shown to mediate adaptation for phase precession in hippocampal neurons (Orban et al., 2006; Kwag et al., 2014), spiking reliability in insect neurons (Gabbiani and Dewell, 2018) and also to maintain regular firing in robust nucleus of acropallium in zebra finches (Hou et al., 2012). Thus FXS mutations, through their effects on potassium channels, may lead to several of the observed network dysfunctions in FXS models.

In the present study, we tested alterations in intrinsic properties of the cell that might underlie the above network observations of uncorrelated activity. First, we observed that cells from FXS knockout (KO) hippocampal slices were more unreliable both at within cell and between cell level, than controls. Consistent with the developmental manifestations of FXS, this effect was absent in juvenile mice and emerged only after ~6 weeks. Decreased spiking in KO mice was correlated with increased variability. At the mechanistic level, we found that the spiking changes were due to elevated medium AHP (mAHP) which in turn was due to elevated SK currents. In contrast to these observations of decreased spiking in the CA1 region of adult animals, we observed increased spiking in the CA3 region of juvenile animals

153 (as seen in Deng et al., 2019) but not in CA1. We did not see any significant change
154 in spatial distribution of SK channels either in CA3 or CA1, in either juvenile animals
155 or in adult animals. This too is consistent with earlier observations (Deng et al.,
156 2019). Finally, we tested the outcome of blockers of SK and found that that they
157 indeed led to a partial rescue of the observed phenotype of increased spiking
158 variability in adult animals.

159

160 **Materials and Methods**

161 **Animals**

162 C57BL/6 strain of *Fmr1tmCgr* male mice were used for the experiments. All
163 experimental procedures were approved by the NCBS ethics committee (Project ID:
164 NCBS-IAE-2017/04(N)). The animals were housed in the institute animal house
165 where they were maintained in 12 hr light and 12 hr dark cycle. The animals used
166 older animal group was in the range of 6-8 weeks of age, and the younger group was
167 3-4 weeks old.

168 **Slice preparation**

169 Mice were anaesthetized with halothane. Their head was decapitated after they were
170 euthanized by cervical dislocation. Hippocampal slices were made in the ice cold
171 aCSF of the composition: 115 mM NaCl, 25 mM glucose, 25.5 mM $NaHCO_3$,
172 1.05mM NaH_2PO_4, 3.3mM KCl, 2mM $CaCl_2$, and 1mM $MgCl_2$. 400µm thick slices
173 were made using a VT1200S vibratome and then incubated at room temperature for
174 1 hour in the aCSF, which was constantly bubbled with 95% O_2 and 5%CO_2.
175 Subsequently, the slices were transferred to the recording chamber where they were
176 maintained at an elevated temperature of 30ºC-34ºC for the recordings.

177 **Electrophysiology**

178 CA1 neurons were identified under an upright DIC microscope (Olympus BX1WI
179 microscope) using a 40X objective (water immersion lens, 0.9 NA LUMPLFLN, 40X).
180 2-4 MOhm pipettes were pulled from thick walled borosilicate glass capillaries on a
181 P-1000 Flaming micropipette puller (Sutter instruments). The pipettes were filled with
182 internal solution of the following composition for whole cell Current Clamp
183 recordings: 120mM potassium gluconate, 20mM KCl, 0.2mM EGTA, 4mM
184 NaCl,10mM HEPES buffer, 10mM phosphocreatine, 4mM Mg-ATP, and 0.3mM Na-
185 GTP (pH 7.4, 295 mOsm). For Voltage Clamp recordings, the same composition of
186 internal solution was used with the one change that 120mM potassium gluconate
187 was substituted with 120mM potassium methylsulphate. Cells were recorded if they
188 had a resting potential <-60mV. We also required that they exhibit stable firing with
189 little or no depolarization block for lower current inputs. Series resistance and input
190 resistance were continuously monitored during the protocols and the cell was
191 discarded if these parameters changed by >25%.

192

193 **Protocol for measuring spike variability and analysis**

194 All spike variability and precision experiments were done in current clamp mode. A
195 step input current stimulus of 150pA DC for 900 ms was used for the majority of the
196 recordings. In some cases, as indicated in the text, frozen noise and sinusoidal input
197 currents were also used, riding on a baseline current step of 150pA, and again for a
198 duration of 900 ms. SD of noise used in noise protocols were 10pA, 25pA, 50pA and
199 100pA with a time-cutoff of τ=3msec. For sinusoidal currents SD of 50pA and 100pA
200 were used at 5 Hz. All the protocols were repeated for 25 trials. Within-cell spike

201 variability (CV_w) was computed as Coefficient of Variation (CV) in spike numbers
202 across 25 trials. Spike numbers computed for all 25 trials were used to find the
203 Standard Deviation in spike numbers which was then divided by mean number of
204 spikes to find CV_w.

205 $$(CV_w)_n = \sigma_n/\mu_n \qquad \text{Equation 1.}$$

206 Where *n* is the cell index, σ_n is the standard deviation across trials within cell *n*, and
207 μ_n is the mean number of spikes across all the trials within cell *n*.

208 The vector CV_w was computed for all recorded KO and WT cells respectively, and
209 used for comparing the responses (Fig 1E). The distributions in CV_w were compared
210 using the Wilcoxon test.

211 The analysis of CV_b was derived from a paper which reports experiments on network
212 synchrony (Talbot et al., 2018). In contrast to our CV_w analysis where variability in
213 spiking was assessed within each cell, in CV_b we measure across trials between
214 cells. For computing between-cell spiking variability (CV_b), spike numbers on
215 corresponding trial numbers were compared between different cells. Specifically, we
216 constructed a vector for each cell whose entries were the number of spikes for
217 successive trials. These vectors were compared across different cells, within the
218 same genotype and used to find CV_b. The following formula was used for the
219 computation:

220 $$(CV_b)_i = \sigma_i/\mu_i \qquad \text{Equation 2.}$$

221 Where *i* is the trial index, σ_i is the standard deviation over trial *i* between cells, and μ_i
222 is the mean number of spikes on trial *i*, between all cells. The CV_b vectors were
223 computed for WT and KO populations respectively (Figure 1F) and compared using
224 Wilcoxon statistics.

225

226 **Measurement of spike timing precision: CV_s**

227 Spike times were found for all the spikes in all trials. The Inter Spike Interval (ISI)
228 was computed for the first two spikes and for spikes that bracketed a time of 500ms
229 after the start of the step input protocol. For each cell *m* we obtained the Coefficient
230 of variation, CV_{s0_m} and CV_{s500_m} for the first ISI and the ISI at 500 ms, respectively:

231 $$CV_{s0_m} = \sigma_{0m}/\mu_{0m} \qquad \text{Equation 3.}$$

232 Where *m* is the cell index, σ_m is the standard deviation of ISI across trials within cell
233 *m*, and μ_m is the mean ISI across all the trials for cell *m*. We calculated CV_{s500_m} in a
234 similar manner.

235 By repeating this calculation over all cells, we obtained the following four vectors:
236 CV_{s0_WT}, CV_{s500_WT}, CV_{s0_KO}, and CV_{s500_KO}. The distributions in these four vectors
237 were compared using a two-way ANOVA.

238 **Measurement of spike timing precision: Jitter Slope**

239 The jitter slope analysis was taken from (Bacci and Huguenard, 2006). Jitter was
240 defined as σ_{ti}, which is the standard deviation of spike timing for spike number *i*,
241 compared over all trials for a given cell. In this manner the vector σ_t was obtained by
242 considering all the spike numbers. Note that not all trials had the same number of
243 spikes, so the final few spike numbers may have had fewer samples in σ_t.(Extended
244 figure 1-1).

245 The Jitter slope was obtained as a regression fit for the vector σ_t , with the x axis
246 defined by the corresponding vector for mean timings μ_t. This slope was calculated
247 for spikes falling in the last 400 ms of the current pulse since this is where the SK

248 channel is activated. As a pre hoc criterion, cells were required to have a minimum of
249 two spike time points in order to be selected for this calculation. Note that this
250 criterion excluded several cells which had strong suppression of firing towards the
251 end of the trial, presumably due to SK channel activation. Thus this measure was
252 compromised by being insensitive to precisely those cells with the largest effects in
253 the KO.

254 (Extended data 1-1)

255 **Measurement of fI curves**

256 The measurement of f-I curves was done in current clamp. For plotting f-I curves,
257 each cell was given input currents from -100pA to 400pA at its resting membrane
258 potential. The mean ± SEM of the number of spikes elicited for each input current
259 was plotted on the Y axis, and the corresponding input current on the X axis.

260 **AHP measurement**

261 AHPs were measured by holding the cell at -70mV in Current Clamp mode, using
262 some holding current. In each trial, the holding current was set to zero for 200msec
263 and then step input for 100msec was delivered. The current during this step input
264 was adjusted so that the cell produced 5 spikes in 100msec. This stimulus was
265 repeated for 15 trials and the voltage traces of all the trials were averaged. AHPs
266 were analyzed as the hyperpolarization after the spike train. mAHP was computed
267 as the average hyperpolarization 50msec after the spike train, and sAHP was
268 computed 200msec after the spike train (Fig 5A and 5B).

269 **Immunofluorescense experiments and analysis**

270 3-4 week or 6-8 week old animals were anaesthetized and brains were dissected
271 out. Brains were fixed in 4%PFA for 48hrs at 4°C. Post fixation, brains were washed
272 with PBS and 30 µm thick slices were cut on a VT12000S vibratome. Slices were
273 kept in cryoprotectant solution and stored at -20°C for further use. Slices were re-
274 suspended in Phosphate Buffer Saline (PBS) solution for the experiment. 50mM
275 Ammonium Chloride (NH_4Cl) was used to quench auto fluorescence from the
276 samples. After multiple steps of washing and permeabilization with 0.3% PBS with
277 Triton-X 100, cells were incubated with 5% Normal Goat Serum (NGS) for blocking
278 for 1-2 hr. Followed by washes, slices were incubated in primary antibody for SK2
279 channel, overnight at 4°C. Primary antibody was purchased from Alomone Labs (Cat
280 # APC–028) and were used in 1:300 dilution with 2.5% NGS. Further, slices were
281 incubated in secondary antibody at 1:500 dilution for 1-2 hrs at room temperature.
282 Followed by several washes and DAPI stain (Sigma) for 15 mins in PBS, slices were
283 mounted in Prolong Gold mounting media and imaged in Olympus FV3000 confocal
284 microscope.

285 **Measurement of M and I_h currents**

286 For measuring Ih sag produced in voltage change, cells were held at -70mV
287 and given a step hyperpolarization of 250pA for 500msec, in current clamp mode.
288 Voltage deflection was calculated by the finding the percentage change between
289 maximum and steady state voltages during the hyperpolarizing pulse ((V_{max}-
290 V_{ss})/V_{max})/100. Each cell was presented with 15 trials and I_h sag was averaged
291 across all the trials to get a value for a cell.

292 TTX (0.5 µM) was added in the bath while measuring M currents in voltage-
293 clamp. For measuring M currents, cells were held at -20mV and M currents were

294 deactivated in steps from -20mV to -80mV in difference of 10mV of 900msec time
295 duration. Difference between steady state current after the start of the protocol (from
296 the last 250msec) and baseline of the cell was quantified as the current elicited due
297 to the protocol. Specific M current blocker XE991 (30μM) was perfused to get post
298 blocker trace. Difference between Pre and Post XE991 was quantified as M current.

299

300 **Measurement of SK currents**

301 TTX (0.5 μM) was added in the bath while measuring SK currents in voltage-clamp.
302 For measuring SK currents cells were held at -55mV while increasing voltage steps
303 were given from -55mV to +35mV, in increments of 10mV, for 800msec duration.
304 Each voltage step was preceded with a small hyperpolarization from -55mV to -
305 65mV for 100msec. Cell capacitance compensation was done during the recordings.
306 The SK currents were estimated from the amplitude of the outward current 25 ms
307 after the voltage was returned to the holding potential as the initial part of the trace
308 will be contaminated with capacitance currents (Figure 6A and 6B). Apamin
309 perfusion (100nM) was done to identify these currents. Same protocol was used post
310 apamin perfusion. The difference current of pre apamin and post apamin was
311 quantified to find apamin sensitive SK current.

312 **Data acquisition and Analysis**

313 Recordings were done using an Axopatch 200 B amplifier and digitized using
314 Digidata 1400A. Current clamp recordings were filtered at 10 KHz and sampled at 20
315 KHz. Voltage Clamp recordings were carried out at a gain of 5, filtered at 3 KHz,
316 sampled at 20 KHz. All analysis was done using custom written code in MATLAB
317 (R2013a) and Graph Pad Prism 6. Statistical tests were done after checking the

318 normality of the data. We plotted the data to check for normality. Even if the data
319 looked normal, Wilcoxon rank sum test was used for most analysis for more stringent
320 results. For multiple comparisons ANOVA was used with Sidak's post hoc test or t-
321 test with Bonferroni correction as post hoc tests. All the data is plotted as mean ±
322 SEM.

323 **Drugs and Chemicals used**

324 All toxins were purchased from Sigma other than TTX which was from Hello Bio.
325 TTX (Stock of 0.5mM) and apamin (Stock solution of 1mM) were made in milliQ
326 water. XE991 (Stock 10mM) was made in DMSO. All stocks were stored at -20° C
327 and were diluted to the working concentration immediately before the experiments.

328 **Experiment design and statistical analysis**

329 We have used hippocampal slice preparation from male mice in this study, where
330 CA1 and CA3 regions were used for electrical recordings. Different current inputs
331 were injected into the cell soma via recording electrode and elicited spikes were
332 recorded in current clamp mode. Spiking variability was assessed by finding
333 Coefficient of Variation (CV) for within cell and between cells. Spike precision was
334 assessed by finding slope of Standard deviation in spike times over multiple trials.
335 SK currents were measured in voltage clamp and were found to be partially
336 responsible for increased variability. All analysis and plotting was done in MATLAB
337 and GraphPad 6. Normality of the data was checked by plotting it. Even if the
338 distribution followed a normal distribution profile, Wilcoxon test was used. For
339 multiple comparisons 2- way or 3- way ANOVA with Sidak's post hoc test or t-test
340 using Bonferroni correction were used as post hoc test.

341

342

343 **RESULTS**

344

345 **FMR1 KO cells exhibit increased variability in spike numbers and impaired**
346 **spike precision**

347

348 We performed whole cell patch clamp recordings in brain slices from CA1 cells of
349 dorsal hippocampus in male wild-type (WT) and KO littermate animals (6-8weeks
350 old). Somatic current injection was used to inject various waveforms of current (Fig
351 1A). These included a square current step, frozen noise riding on a current step, and
352 a sinusoidal waveform riding on a current step (Fig 2). In each case we measured
353 the variability in spiking over the 900 ms of current injection, in two respects: first, the
354 variability within a neuron, over repeated trials (CV_w), and second, the variability
355 between neurons, comparing matching trials between cells (CV_b) (methods).

356 We computed the co-efficient of variation (CV_w) of spike numbers for each of the
357 current stimulus protocols (methods). We observed that the CV of spike numbers
358 across trials within cells (CV_w) was significantly higher for KO cells as compared to
359 WT, but only for the step current protocol (CV_w for WT 0.038 ± 0.005, n=30 cells;
360 CV_w for KO 0.057 ± 0.006, n=29 cells; p=0.0048, Wilcoxon rank sum test) (Fig 1B,
361 1C,1D,1E). For other protocols, where frozen current noise or sinusoidal waveforms
362 were riding on top of a current pulse, spikes were very reliable over different trials for
363 both WTs and KOs (Fig 2A, Fig 2B, Fig 2C, Fig 2D and Fig 2E). We then estimated
364 the variability between cells (CV_b). To do this, we compared spike numbers between
365 different cells of WT and KO by matching corresponding trials, such that we
366 compared spiking between the first trials of WT between all the WT cells, second

367 trials of WT between all cells and so on forth, within the same genotype. Similar
368 comparisons were made for KO cells as well (methods). From this procedure we
369 found that between cell variability was significantly elevated in KO cells as compared
370 to WT (CV_b for WT cells 0.29 ± 0.003, n=30 cells; CV_b for KO cells 0.41 ± 0.002,
371 n=29 cells; p<0.001; Wilcoxon rank sum test) (Fig 1F).We plotted the CV_w of spike
372 numbers within the cell, for WT and KO population and observed that KOs have
373 much wider spread as compared to WT (SD of the CV_w population for WT cells =
374 0.026, n=30 cells; SD of the CV_w population for KO cells = 0.03, n=29 cells) (Fig 1G
375 and 1H). This implied that KOs have a more heterogeneous population than WT
376 cells. In KO mice, some cells were reliable, i.e., they produced a similar number of
377 spikes across multiple trials but some did not. Based on this analysis (Fig 1G and
378 1H) we found that 51.7% of KO cells had CV_w values which did not overlap with
379 those of WT cells.

380 Spike timing precision was computed by finding CV_s in inter-spike intervals
381 (ISIs, methods). We compared CV_{s0} with CV_{s500} to assess the contribution of SK
382 channels, which are shut at t=0, but open by t=500. We chose not to use the last ISI
383 for this comparison because the timing of the last spike was very variable in KO
384 cells. We then compared CV_s at t=0 and t=500, between WT and KO cells using 2-
385 way ANOVA. We found that there was no significant difference in between WT and
386 KO for CV_{s0}. However, at t=500, we found that CV_{s500_KO} was significantly elevated
387 compared to CV_{s500_WT} (CV_{s0_WT} = 0.11 ± 0.014; CV_{s0_KO} = 0.09 ± 0.007; CV_{s500_WT} =
388 0.13 ± 0.01; CV_{s500_KO} = 0.23 ± 0.03; $F_{(1,113)}$ =5.78; p=0.018 for WT vs KO
389 differences; two-way ANOVA) (Fig 1J)

390 Increased within cell (CV_w), between cell (CV_b) variability of spike numbers and
391 increased CV_s of spike timings are both indicative of abnormal coding in KO

392 neurons. Thus these initial recordings showed that there was increased

393 heterogeneity in spiking in CA1 pyramidal neurons of KO mice.

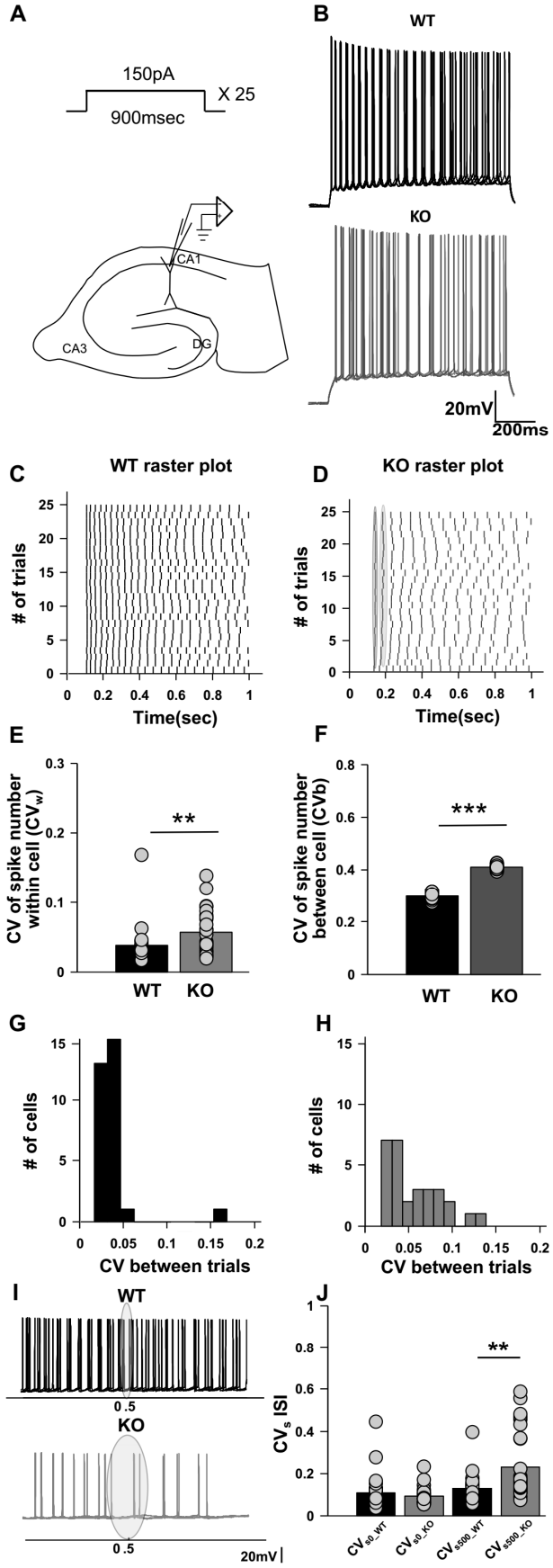
A
150pA
X 25
900msec
CA1
CA3
DG
B
WT
KO
20mV
200ms
C
WT raster plot
# of trials
Time(sec)
D
KO raster plot
# of trials
Time(sec)
E
CV of spike number within cell (CVw)
**
WT
KO
F
CV of spike number between cell (CVb)
***
WT
KO
G
# of cells
CV between trials
H
# of cells
CV between trials
I
WT
KO
0.5
20mV
J
CVs ISI
**
CVs0_WT
CVs0_KO
CVs500_WT
CVs500_KO

394

395 **Figure 1. Increased spike variability and spike timing imprecision both at**
396 **within cell level (CV_w) across multiple trials and between cells (CV_b) in CA1**
397 **hippocampus of FXS animals.**

398 (A) Schematic of a hippocampal slice and the step depolarization protocol. The
399 protocol consists of a 150pA step for 900msec time duration repeated over 25 trials.

400 (B) Representative raw traces of spiking, superimposed for four trials only for WT
401 (black) and KO (grey). Scale bar 20mV, 200msec.

402 (C) Representative raster plot showing spiking for the step depolarization protocol
403 for WT (black) and (D) KO (grey). Also showing the methodology for computing jitter
404 slope for estimating spike timing precision, further plotted in 1I and 1J.

405 (E) Bar plot for within cell variability across multiple trials (CV_w) WT (n=30 cells,
406 black) and KO (n=29 cells, grey). KO cells have significantly higher within cell
407 variability than WT cells (p=0.0048, Wilcoxon rank sum test).

408 (F) Bar plot for between cell variability (CV_b) for matched trials, WT (n=30 cells,
409 black) and KO (n=29 cells, grey). KO cells have significantly higher between cell
410 variability than WT cells ($p<0.001$, Wilcoxon rank sum test)

411 (G) Histogram showing spread of CV_w parameter for WT (n=30 cells, black) and (H)
412 for KO (n=29 cells, grey). KO cells have more spread in CV_w parameter, depicting
413 heterogeneity in KO cell population.

414 (I) Representative trace showing the time window where CV_s in ISI is calculated for
415 WT (upper black trace) and for KO (lower grey trace). Superimposed traces are for
416 four trials only. Scale bar 20mV.

417 (J) Bar plot for CV_s in ISI, a measure of spike precision for WT (n=30 cells, black)
418 and KO (n=29 cells, grey). CV_{s0} is not significantly different between WT and KO.
419 However, there is a significant increase in the CV_{s500} for KO cells as compared to
420 WT (p=0.018 for WT vs KO differences; two-way ANOVA

421 **KO mice exhibit increased variability in spike number between cells (CV_b) for**
422 **frozen noise stimuli**

423 Neuronal coding takes place against a noisy background of continuous synaptic
424 input (Faisal et al., 2008). Frozen noise stimuli have therefore been used in several
425 studies to examine single-neuron computations and are considered more
426 physiological (Stevens and Zador, 1998; Carandini, 2004; Fujisawa et al., 2004; Han
427 and Boyden, 2007). We injected noise waveforms in the soma using a design similar
428 to that of Mainen and Sejnowski, 1995. The stimulus waveforms were mainly either
429 of random noise or sinuosoidal input currents (for details see methods). The resting
430 Vm was controlled by maintaining constant current injection into the cell while
431 recording. Cells were only accepted if the fluctuations in their potential while
432 recording were smaller than ± 2.5mV. For noisy inputs, spikes across multiple trials
433 aligned very precisely for both WT (Fig 2A, 2C) and KO cells (Fig 2B, 2D). Upon
434 computation of CV of spike numbers across trials within cell (CV_w), there were no
435 statistically significant differences for any of the protocols (Fig 2E). However,
436 between cell variability differences (CV_b) were still significantly elevated for KO cells,
437 for all stimulus protocols (Fig 2F). We did three way ANOVA for all the protocols on
438 the no of spikes produced in respective protocols for WT and KO. The 3 factors
439 were: across trials, across cells and WT vs. KO. ANOVA results were significant for
440 across cells ($p<0.001$), for WT vs. KO ($p<0.001$) but not for across trials ($p=1$) for all
441 the protocols. Thus, between cell variability (CV_b) reveals robust phenotypic

differences which are also observed between WT and KO for the input noise stimulus. The same is not true for across trials within cell (CV_w) differences.

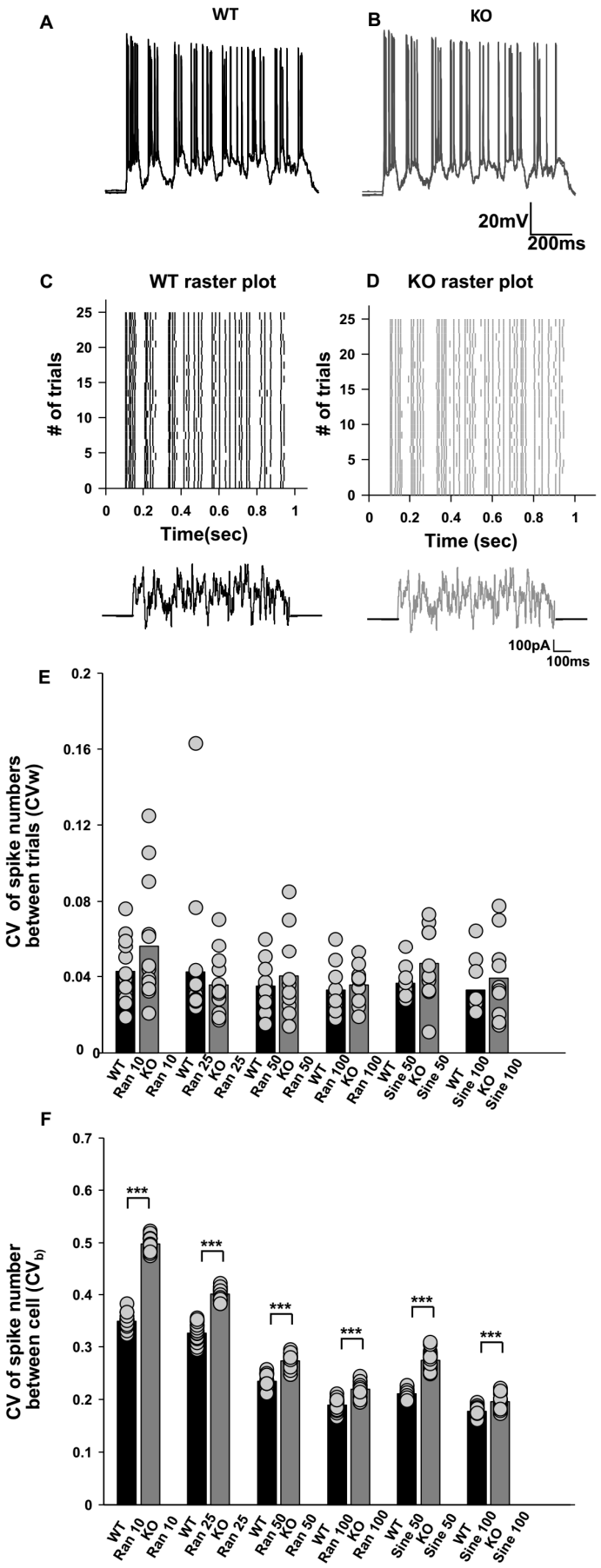
A
WT
B
KO
20mV
200ms
C
WT raster plot
D
KO raster plot
# of trials
Time(sec)
Time (sec)
100pA
100ms
E
CV of spike numbers between trials (CVw)
F
CV of spike number between cell (CVb)
***
WT
Ran 10
KO
Ran 10
WT
Ran 25
KO
Ran 25
WT
Ran 50
KO
Ran 50
WT
Ran 100
KO
Ran 100
WT
Sine 50
KO
Sine 50
WT
Sine 100
KO
Sine 100

444

445 **Figure 2. KO cells have increased spike variability between cells (CV_b) for**
446 **noise and sinusoidal stimuli but not for within cell variability (CV_w) across**
447 **trials.**

448 (A) Representative raw plot of spiking showing no spike variability or spike precision
449 differences for Ran 100 noise protocol across multiple trials for WT(black) and (B)
450 for KO (grey). The trace is for four superimposed trials. Scale bar 20mV,
451 200msec.

452 (C) Raster plot showing no spike variability or spike precision differences for Random
453 100 noise protocol across multiple trials for WT(black) and (D) for KO (grey). Trace
454 below indicates Ran 100 input protocol. Scale bar 100pA, 100msec

455 (D) Bar plot for within cell variability differences (CV_w) for all noise and sinusoidal
456 protocols for WT (black bars) and KO (grey bars). The protocol is numbered by the
457 standard deviation (SD) in pA (random protocols) or sine-wave amplitude (sine
458 protocols) (Random 10 protocol: n=16 for WT and n=13 for KO; Random 25: n=16
459 for WT and n=13 for KO; Random 50: n=10 for both WT and KO; Random 100:
460 n=10 for both WT and KO; Sine 50: n=10 for both WT and KO; Sine 100: n=10 for
461 both WT and KO; error bar represent SEM). No significant within cell variability
462 (CV_w) differences were seen between WT and KO in any protocol.

463 (E) Bar plot for between cell variability differences (CV_b) for all noise and sinusoidal
464 protocols (Random 10: n=16 for WT and n=13 for KO; Random 25: n=16 for WT
465 and n=13 for KO; Random 50: n=10 for both WT and KO; Random 100: n=10 for
466 both WT and KO; Sine 50: n=10 for both WT and KO; Sine 100: n=10 for both WT
467 and KO). Significant differences were seen ($p < 0.001$; three-way ANOVA, error
468 bar represent SEM) for all pairs.

469 **Spike imprecision diverges between KO and WT only in adult mice**

470 Fragile X is known to have an age dependent effect where some disease
471 phenotypes get worse with age (Larson, 2005; Cornish et al., 2008; Choi et al.,
472 2010). We asked if similar effects of age might manifest in the phenotype of firing
473 imprecision of KO cells. We therefore repeated our experimental protocols in young
474 (3-4 week old) male WT and KO littermate mice. Regular spike firing was observed
475 in both KO and WT cells for step input current injection (Fig 3A and 3B). As before,
476 we assessed variability of spike numbers across multiple trials for within the cell
477 (CV_w).There was no significant difference between WT vs. KO in these younger mice
478 (CV_w for WT 0.041 ± 0.006, n=26 cells; CV_w for KO 0.03 ± 0.002,n=19 cells; p=0.81;
479 Wilcoxon rank sum test) (Fig 3A,3B,3C,3D and 3E). Spike precision was assessed
480 as above, by finding CV_s of ISI. By this measure too, no significant difference in
481 precision of spike timings was found for KO as compared to WT (CV_{s500} for ISI for
482 WT younger 0.133 ± 0.02, n=26 cells; CV_{s500} for ISI for KO younger 0.103 ± 0.01,
483 n=19 cells; p=0.82, Wilcoxon rank sum test) (Fig 3F). We used a two way ANOVA
484 interaction model for assessing age-dependent differences in spiking variability
485 across different trials in a cell (CV_w) ($F_{(1, 100)} = 4.97$, p=0.028 for WT and KO
486 differences; $F_{(1, 100)} = 8.05$, p=0.005 for interaction factor; two-way ANOVA with
487 interaction model) (Fig 3E). We also estimated differences in spike timing precision
488 across different trials in a cell (CV_{s500}) ($F_{(1, 99)} = 7.47$, p=0.007 for age factor, $F_{(1, 99)}$ =
489 9.46, p=0.003 for interaction factor; two-way ANOVA with interaction model) (Fig 3F).
490 ANOVA indicated a significant interaction between the two factors: age and
491 genotype of the animal. Using post hoc tests we concluded that for KO cells there is
492 a worsening of phenotype for both variability in spiking number (CV_w) across multiple
493 trials within a cell and in spike timing precision (CV_{s500} of ISI) across multiple trials

494 within a cell (Fig 3E and 3F, detailed statistics shown in table 1). However, the same
495 was not seen in WT cells. A two-way ANOVA was done on the number of spikes
496 produced in the 900msec stimulus period used in the step depolarization protocol
497 (Fig1A). In this ANOVA the two factors were: young vs old animals and WT vs. KO.
498 There was no significant change between ages of the animals for both WT and KO
499 ($F_{(1, 101)} = 0.21$; p=0.6) but there was a significant reduction in spike number for KO
500 animals as compared to WT ($F_{(1, 101)} = 5.5$; p=0.021) (Fig 3G). However, the
501 frequency-vs.-current (f-I) curves were not significantly different between WT and KO
502 either in the older (8 weeks) or younger (4 weeks) age groups, when slope of the f-I
503 curves (gain) was used as a readout (Mean gain for f-I curve older WT 0.16 ± 0.007
504 spikes. s^{-1} . pA^{-1} , n= 27 cells; mean gain for f-I curve older KO 0.16 ± 0.008 spikes.
505 s^{-1} . pA^{-1}, n= 25 cells; Mean gain for f-I curve younger WT 0.133 ± 0.01 spikes. s^{-1} .
506 pA^{-1}, n=26 cells; mean gain for f-I curve younger KO 0.136 ± 0.013 spikes. s^{-1} . pA^{-}
507 ^{1}, n=19 cells; $F_{(1, 94)} = 0.03$; p=0.86 for WT and KO differences, two way ANOVA)
508 (Fig 3I and 3J).When comparisons were made of f-I curves of WT and KOs cells,
509 there was reduced excitability seen for some input currents in older animals (Mean #
510 of spikes for input current 125 pA in WT animals 22.07 ± 1.74; n=27 cells; Mean # of
511 spikes for input current 125 pA in KO animals 15.92 ± 2.1; n=25 cells; $F_{(1, 1070)}$ =
512 31.03, p<0.001; two *way* ANOVA) (Fig 3L), but not in younger animals (Mean # of
513 spikes for input current 125 pA in WT animals 21.8 ± 2.9; n=26 cells; Mean # of
514 spikes for input current 125 pA in KO animals 22.8 ± 2.9; n=19 cells, $F_{(1, 923)} = 0.92$;
515 p=0.33; two *way* ANOVA) (Fig 3K). Other properties like spike threshold were not
516 significantly different between WT and KO (Spike threshold for the 1st spike WT -53.6
517 mV ± 0.56 n=30 cells; spike threshold for 1st spike KO -53.8 mV ± 0.62, n=29 cells;
518 Spike threshold for the last spike WT -41.9 mV ± 0.66, n=30 cells; Spike threshold

519 for the last spike KO -43.5 mV ± 0.66, n=29 cells, $F_{(1, 115)} = 1.98$; p=0.16; two way
520 ANOVA). The spread in number of spikes produced by KO neurons was greater than
521 observed in WT, further substantiating the point of increased variability in KO
522 neurons (SD of spike numbers WT = 7.2; n=750 spikes from 30 cells 25 trials each;
523 SD of spike numbers KO = 8.1; n=725 spikes from 29 cells 25 trials each)(Fig 3H).
524 We performed a 3-way ANOVA in which the factors were: across trials, across cells,
525 and WT vs. KO for older age group data. The ANOVA results were highly significant
526 for variability in spike numbers between cells (CV_b) ($F_{(29, 1420)} = 32.04$, $p<0.001$) and
527 differences in spike numbers between WT and KO for older animals ($F_{(1, 1420)} =$
528 209.9, $p<0.001$) but across-trial comparisons did not exhibit a significant difference
529 ($F_{(24, 1420)} = 0.15$, p=1).Thus, there is increase in spike variability with lowered spiking
530 precision for adult KO mice as compared to juvenile KO mice. This divergence
531 which is observed for KO animals with age does not happen for WT animals.

532

533

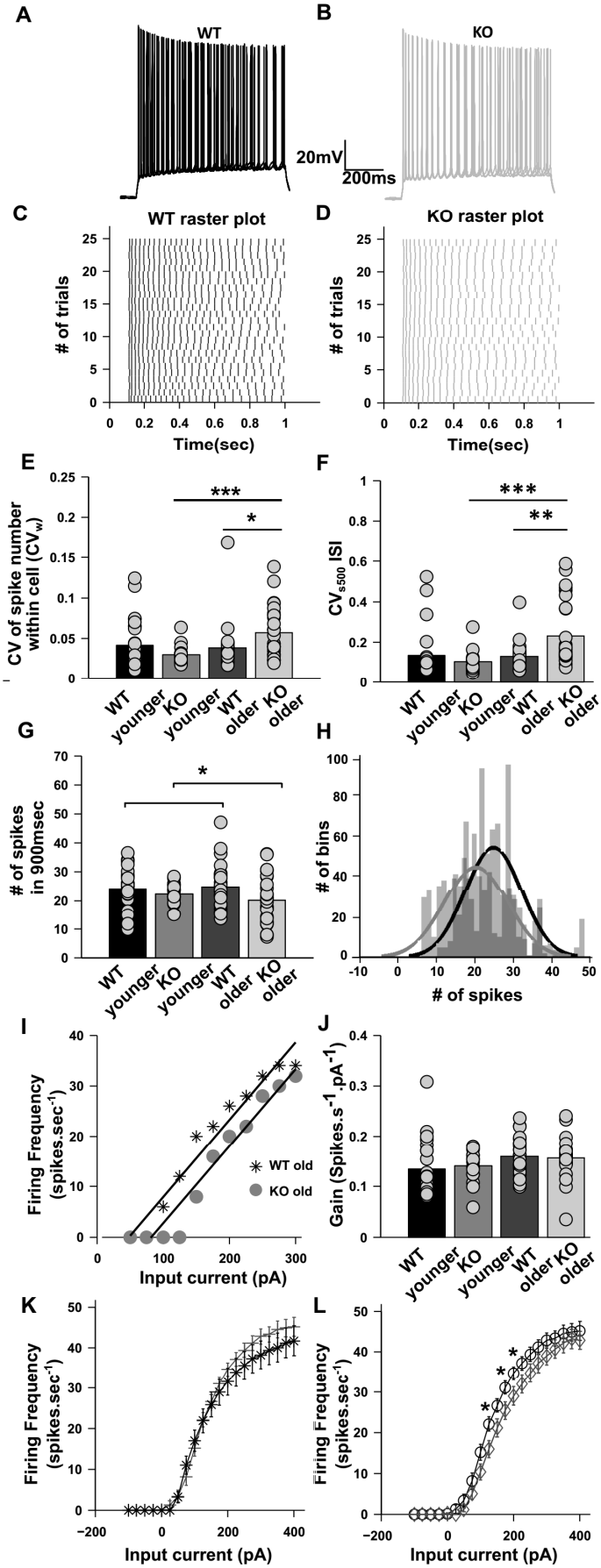
A
WT
B
KO
20mV
200ms
C
WT raster plot
# of trials
Time(sec)
D
KO raster plot
# of trials
Time(sec)
E
CV of spike number within cell (CVw)
***
*
WT younger
KO younger
WT older
KO older
F
CVs500 ISI
***
**
WT younger
KO younger
WT older
KO older
G
# of spikes in 900msec
*
WT younger
KO younger
WT older
KO older
H
# of bins
# of spikes
I
Firing Frequency (spikes.sec-1)
WT old
KO old
Input current (pA)
J
Gain (Spikes.s-1.pA-1)
WT younger
KO younger
WT older
KO older
K
Firing Frequency (spikes.sec-1)
Input current (pA)
L
Firing Frequency (spikes.sec-1)
Input current (pA)

534

535 **Figure 3. Spiking variability and spike imprecision diverges in adult KO**
536 **animals as compared to younger KO but not in WT.**

537 (A) and (B) Representative raw traces of spiking, superimposed for four trials only for
538 WT younger (black) and KO younger (grey). Scale bar 20mV, 200msec.

539 (C) and (D) Representative Raster plots showing spiking for the step depolarization
540 protocol for WT younger (black) and KO younger (grey). Spikes align precisely and
541 have low within cell variability (CV_w) across trials for KO younger as compared to WT
542 younger.

543 (E) Bar plot for comparing within cell variability (CV_w) across multiple trials between
544 WT younger (n=26 cells, black), KO younger (n=19 cells, grey), WT older (n=30
545 cells, light black) and KO older (n=29 cells, light grey). Spiking variability significantly
546 increases for KO animals with age but not for WT animals ($p<0.001$, t-test with
547 Bonferroni correction).

548 (F) Bar plot for CV_{s500} for ISI of the step input protocol, a measure of spike precision
549 for all groups as mentioned in (E). Spiking precision significantly decreases for KO
550 animals with age but not for WT animals ($p= 0.0002$; t-test with Bonferroni
551 correction).

552 (G) Comparison of number of spikes produced during the 900msec stimulus period
553 for each of the groups in (E). There is a non significant change in spike number with
554 age in WT or KO ($p=0.6$; two way ANOVA) but there was a significant reduction in
555 spike number for KO animals as compared to WT ($p=0.021$; two-way ANOVA).

556 (H) Superimposed histograms for number of spikes produced for WT older (light
557 grey) and for KO older (dark grey). Solid lines represent Gaussian fitting. The shift in

558 peaks of the histograms shows that there is a greater spread in spike numbers
559 produced in given trials for KO as compared to WT ($p<0.001$; three way ANOVA).

560 (I) Illustrative f-I curves for a representative cell from older (>6 week) WT animals
561 (black stars), and a cell from older KO animals (filled grey circles). The gain (i.e.,
562 slope) for each cell was computed using a regression fit in the roughly linear domain
563 between 50pA to 300pA.

564 (J) Gain computed by fitting a regression line through the f-I curve for each cell as
565 illustrated in (I), for each of the four experimental conditions. The cells were the
566 same as in G. The gains are not significantly different between WT and KO in any
567 age group (n=27 cells for WT older and n=25 cells for KO older; n=26 cells for WT
568 younger and n= 19 cells for KO younger; $F_{(1, 94)} = 0.03$; $p=0.86$ for WT and KO
569 differences; two way ANOVA).

570 (K) f-I curve for younger WT (black stars, n=26 cells) vs younger KO (grey plus, 19
571 cells) CA1 cells. There is no significant difference between WT and KO cells at this
572 age ($F_{(1, 923)} = 0.92$; $p=0.33$ for WT and KO differences; two way ANOVA).

573 (L) f-I curve for older WT (black circles, n=27 cells) vs younger KO (grey diamonds,
574 25 cells) CA1 cells. There is a significant difference between WT and KO cells at this
575 age ($F_{(1, 1070)} = 31.03$; $p<0.001$ for WT and KO differences; two way ANOVA).

576

577 **Differential effect of FMRP KO in different brain regions**

578 Mouse models of FXS are known to exhibit increased excitability (Contractor et
579 al., 2015; Deng and Klyachko, 2016; Luque et al., 2017). In contrast to previous
580 studies, we observed that excitability was reduced in CA1 neurons in adult mice but
581 not in juveniles. Deng et. al. 2019 have observed increased CA3 excitability in
582 juveniles which was in contrast to what is we observed in CA1, namely, that there is
583 no significant effect on excitability of CA1 pyramidal cells at this time point. In order
584 to address this contrasting result, we repeated the protocol from Deng et. al. in our
585 FXS model, and compared outcomes between CA3 and CA1 (Figure 4). In
586 agreement with their study we observed significantly increased spiking in CA3 cells
587 of FXS mice for some of the input holding currents (# of spikes in 60 s for -48mV
588 holding potential for WT 131.9 ± 17.42, n=10 cells; # of spikes in 60 s for -48mV
589 holding potential for KO 186.3 ± 27.27, n=10 cells; $F_{(1, 72)} = 5.35$, p=0.023 for
590 difference between WT and KO; two-way ANOVA) (Figure 4A, 4B). We did similar
591 experiments in CA1 pyramidal cells, using the same protocol as in Figure 4A and B.
592 We did not find any difference in excitability between WT and KO (# of spikes in 60 s
593 for -48mV holding potential for WT 355.58 ± 40.93, n=12 cells; # of spikes in 60 s for
594 -48mV holding potential for KO 358.67 ± 22.56, n=12 cells; $F_{(1, 88)} = 1.06$, p=0.31 for
595 difference between WT and KO, two-way ANOVA) (Figure 4C, 4D). Upon seeing this
596 differential effect of FMRP KO in different regions of hippocampus, we were
597 interested to see if this might be a function of age. Therefore, we recorded similar
598 protocols from CA3 and CA1 of older animals. We found that the hyper-excitability
599 seen in younger CA3 cells, goes away, leading to no significant difference in spiking
600 activity in these cells for WT vs KO (# of spikes in 60 s for -48mV holding potential
601 for WT 313.6 ± 83.8, n=10 cells; # of spikes in 60 s for -48mV holding potential for

602 KO 181.1 ± 54.9, n=10 cells; $F_{(1, 75)} = 1.16$, p=0.28 for difference between WT and
603 KO, two-way ANOVA) (Figure 4E, 4F). In agreement with our previous results as
604 shown in Fig 3, we observed reduced excitability in CA1 KO cells as compared to
605 WT (# of spikes in 60 s for -50mV holding potential for WT 135.6 ± 35.2, n=8 cells; #
606 of spikes in 60 s for -50mV holding potential for KO 54 ± 20.4, n=8 cells; $F_{(1, 59)} =$
607 7.42, p=0.009 for difference between WT and KO, two-way ANOVA) (Figure 4G,
608 4H). Using these experiments, we were able to replicate previous published results
609 of Deng et. al. 2019. In addition, we found that there were contrasting and age-
610 dependent effects of FMRP KO on the spiking properties of CA1 and CA3 pyramidal
611 neurons.

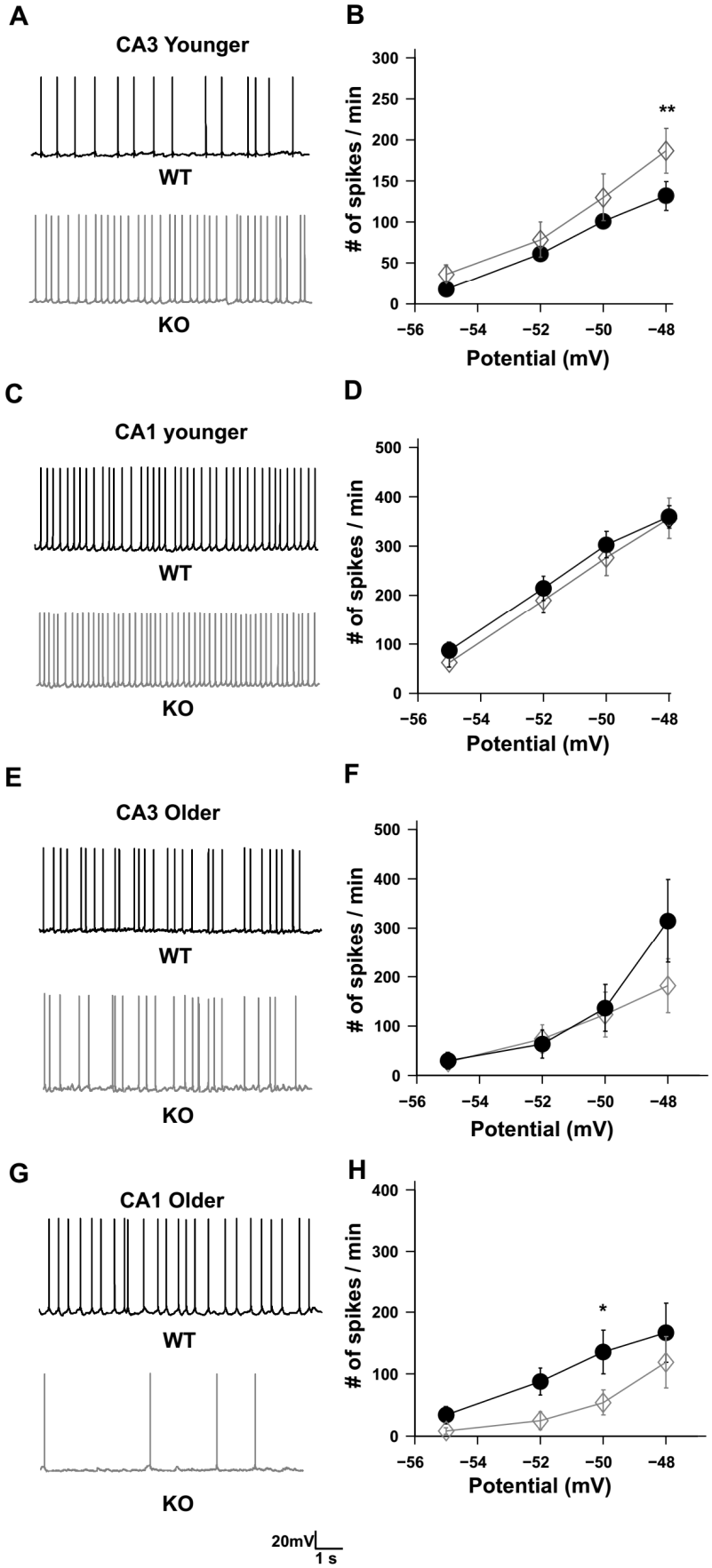
A
CA3 Younger
WT
KO
B
# of spikes / min
Potential (mV)
**
C
CA1 younger
WT
KO
D
# of spikes / min
Potential (mV)
E
CA3 Older
WT
KO
F
# of spikes / min
Potential (mV)
G
CA1 Older
WT
KO
H
# of spikes / min
Potential (mV)
*
20mV
1 s

612

613

614 **Figure 4. Contrasting effects of FMRP KO in different regions of hippocampus**

615 A) Representative traces showing increased excitability between WT (black) and KO
616 (grey) CA3 cells in younger animals. Traces are from the recording where the cells
617 are held at -48mV. Scale bar 20mV, 1s.

618 B) Line plot showing increased excitability for KO CA3 cells (n=10 cells, grey diamond)
619 as compared to WT CA3 cells (n=10 cells, filled black circles), when the cells were
620 held at -48mV, for younger animals. For other holding potentials the spike numbers
621 are not significantly increased for KO cells ($F_{(1, 72)} = 5.35$, p=0.023 for difference
622 between WT and KO, two way ANOVA, error bar represent SEM)

623 C) Representative traces showing no change in excitability between WT (black) and
624 KO (grey) CA1 cells in younger animals. Traces are from the recording where the
625 cells are held at -48mV. Scale bar 20mV, 1s.

626 D) Line plot showing no change in excitability for KO CA1 cells (n=12 cells, grey
627 diamond) as compared to WT CA1 cells in younger animals (n=12 cells, filled black
628 circles) ($F_{(1, 88)} = 1.06$, p=0.31 for difference between WT and KO, two-way
629 ANOVA, error bar represent SEM).

630 E) Representative traces showing no change in excitability between WT (black) and
631 KO (grey) CA3 cells in older animals. Traces are from the recording where the cells
632 are held at -48mV. Scale bar 20mV, 1s.

633 F) Line plot showing no change in excitability for KO CA3 cells (n=10 cells, grey
634 diamond) as compared to WT CA3 cells (n=10 cells, filled black circles), when the
635 cells were held at -48mV, for older animals. ($F_{(1, 72)} = 1.17$, p=0.28 for difference
636 between WT and KO, two way ANOVA, error bar represent SEM)

637 G) Representative traces showing reduced excitability for KO cells (grey) as compared
638 to (black) and KO CA1 cells in older animals. Traces are from the recording where
639 the cells are held at -50mV. Scale bar 20mV, 1s.
640 H) Line plot showing decreased excitability for KO CA1 cells (n=8 cells, grey diamond)
641 as compared to WT CA1 cells (n=8 cells, filled black circles), when the cells were
642 held at -60mV, for older animals. For other holding potentials the spike numbers
643 are not significantly decreased for KO cells ($F_{(1, 59)} = 7.42$, p=0.009 for difference
644 between WT and KO, two way ANOVA, error bar represent SEM)
645

646 **mAHP currents are elevated in older KO animals as compared to WT but no**
647 **significant changes in I_h and M currents**

648

649 We next investigated the mechanisms for increased variability in KO
650 animals, on the basis of the above observations of increased variability and fewer
651 spikes (Fig 3G and 3L) in the later part of the current pulse. In particular, we
652 hypothesized that medium afterhyperpolarization (mAHP) and slow
653 afterhyperpolarization (sAHP) currents were likely candidates to mediate such
654 slower-onset effects. We asked if these currents might be altered in FXS cells.

655 To test this hypothesis we compared AHPs for WT vs. KO in older and
656 younger animals. Cells were held at -70mV to record AHPs. We quantified AHPs by
657 examining the hyperpolarization elicited with a spike train of 5 spikes in 100msec.
658 Hyperpolarization was quantified at mAHP peak (50msec after the spike train) and at
659 sAHP peak (200msec after the spike train). We found that mAHP was elevated only
660 in older KOs but not in younger KOs when compared to their WT littermates (mAHP

661 for WT older -0.26 ± 0.16, n=12 cells; mAHP for KO older -0.71 ± 0.15, n=13 cells;
662 mAHP for WT younger 0.41 ± 0.2, n=14 cells; mAHP for KO younger -1.14 ± 0.5,
663 n=18 cells; $F_{(1, 46)} = 4.8$, p=0.033 for WT and KO differences) (Fig 5C,detailed
664 statistics shown in table 1). We found similar results for sAHP measurements as
665 well. We found that sAHP was significantly elevated only for older KO animals as
666 compared to their WT littermates but not significantly different for younger KO
667 animals as compared to their younger WT littermates (sAHP for WT older 0.006 ±
668 0.1, n=12 cells; sAHP for KO older -0.37 ± 0.11, n=13 cells; sAHP for WT younger
669 0.04 ± 0.12, n=14 cells; sAHP for KO younger 0.047 ± 0.2, n=18 cells; $F_{(1, 54)} = 8.84$,
670 p=0.004 for WT and KO differences) (Fig 5D). As there was no significant difference
671 in spike variability and spike time precision in younger KO animals, we hypothesized
672 that the observed spiking variability in older KO animals might be due to elevated
673 mAHPs, which has a strong change with age in KO animals. Further, the stimulus
674 period used in the previous experiments (Fig 1) was of 900ms which is the peak time
675 of activation for mAHP mediating ion channels.

676 The mAHP in CA1 cells is mediated by I_h, M and SK currents. A previous study
677 has shown that I_h currents are not significantly altered in soma of FXS cells (Brager
678 et al., 2012). M currents are known to affect the Resting Membrane Potential (RMP)
679 and spike adaptation index (Madison et al., 1987; Guan et al., 2011; Nigro et al.,
680 2014; Hönigsperger et al., 2015). Neither RMP nor spike adaptation index were
681 significantly changed in FXS cells, indicating that M currents might not be
682 responsible for the observed phenotype. To further test this idea, I_h currents and M
683 currents were recorded from soma of CA1 cells and compared between WT and KO
684 for adult animals. As there was no difference in mAHP at juvenile stage for KO cells,
685 we did not measure I_h and M currents for them. I_h channel activity was recorded

686 using a hyperpolarization pulse. The voltage sag produced in response to the pulse,
687 was quantified according to a method adapted from Brager and Johnston, 2012
688 (Methods, Fig 5E). As observed previously, there was no significant difference in I_h
689 sag between WT and KO CA1 cells, at somatic level. (% sag for WT 17.7 ± 1.64,
690 n=10 cells; % sag for KO 18.87 ± 2.51, n=10 cells; p=0.91; Wilcoxon rank sum test)
691 (Fig 5F).

692 To measure M currents we used the protocol adapted from Shah et al 2002
693 (Methods). According to the protocol the cells were held at -20mV and M currents
694 were deactivated in steps from -20mV to -80mV. M current specific blocker XE991
695 was used to obtain the post blocker trace. Post blocker trace was subtracted from
696 pre blocker trace to obtain XE991 sensitive M currents (Fig 5G). We found no
697 significant differences in M currents between WT and KO CA1 cells. (Mean M
698 current for step -80mV for WT -40.9 ± 6.33, n=19 cells; Mean M current for step -
699 80mV for KO 45.94 ± 6.87, n=19 cells; $F_{(1, 258)} = 2.54$, p=0.11 between WT and KO,
700 two-way ANOVA) (Fig 5H). Overall, these observations suggest that neither I_h nor M
701 currents contribute to the observed elevation in mAHP in KO animals.

702

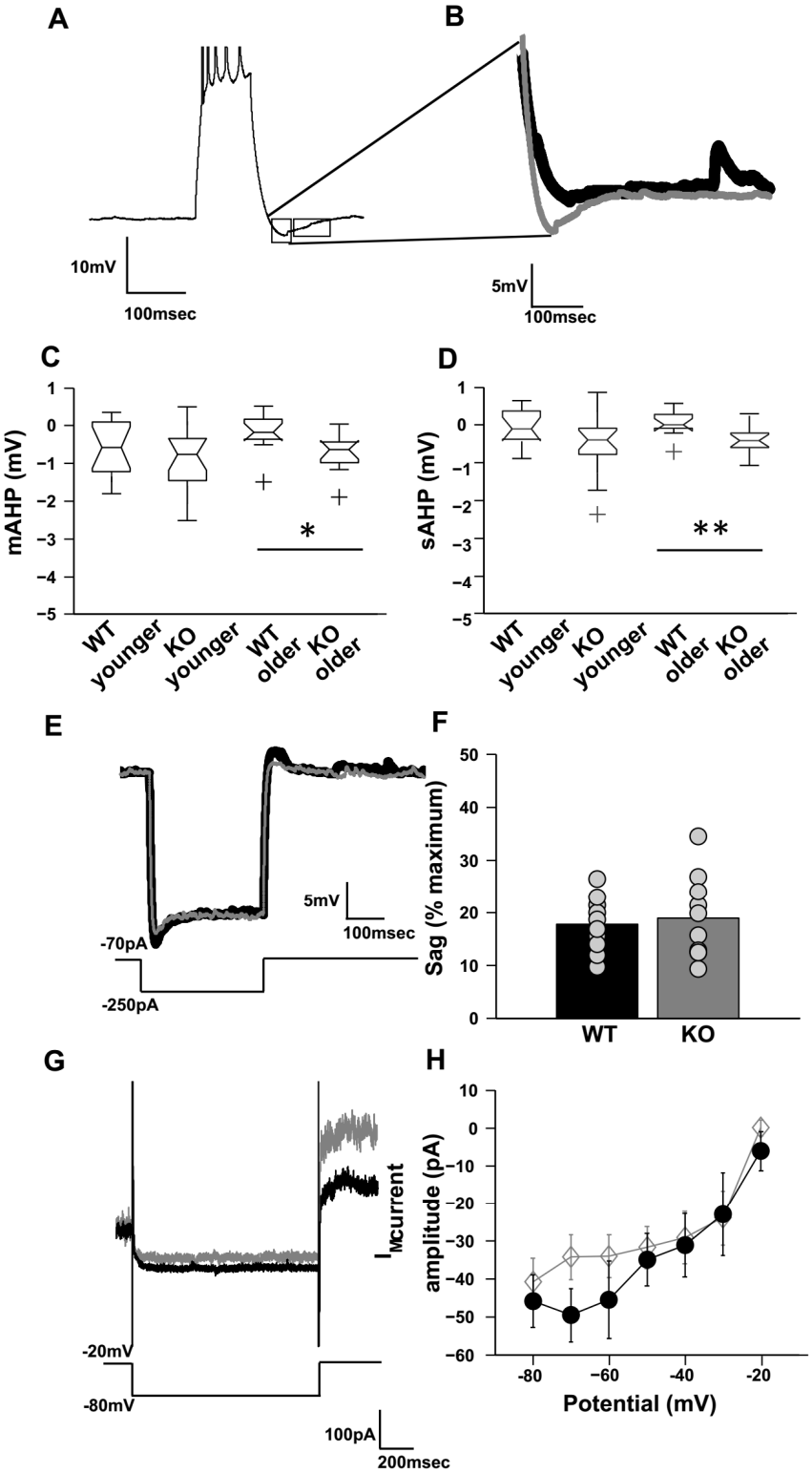

703

704

705 **Figure 5. mAHP and sAHP are elevated in FXS KO neurons**

706 (A) Representative trace for the protocol to measure mAHP and sAHP.
707 Hyperpolarization within 50msec of the spike train (1) is quantified as mAHP while
708 hyperpolarization following the spike train 200msec after the spike train (2) is
709 quantified as sAHP. Scale bar 10mV, 100msec.

710 (B). Superimposed traces of WT older and KO older AHP currents showing elevated
711 mAHP currents for KO cell (grey) as compared to WT cell (black). Scale bar 5mV,
712 100msec.

713 (C) Box plot showing mAHP currents for all groups (n=12 cells for WT older, n=13
714 cells for KO older, n=14 cells for WT younger and n=18 cells for KO younger). mAHP
715 are elevated only for older KO animals vs. older WT (p=0.018; t-test with Bonferroni
716 correction, error bar represent SEM).

717 (D) Box plot showing sAHP currents for all groups (n=12 cells for WT older, n=13
718 cells for KO older, n=14 cells for WT younger and n=18 cells for KO younger). sAHP
719 is elevated for older KO vs older KO (p=0.008; t-test with Bonferroni correction) but
720 not in younger KO vs younger WT animals as well (p=0.06 for sAHP between WT
721 younger and KO younger, error bar represent SEM).

722 (E) Representative trace for the protocol to measure I_h current. Superimposed traces
723 of WT (black) and KO (grey) showing no significant difference in the response. Sag
724 produced in response to 250pA hyperpolarizing pulse was quantified to estimate I_h
725 current. Scale bar 5mV, 100msec.

726 (F) Bar plot for showing % sag produced due to I_h current for WT older and KO older
727 (n=10 cells for both WT and KO older). There was no significant difference in sag
728 due to I_h current (p=0.91, Wilcoxon's test).

729 (G) Representative traces showing XE991 sensitive M current for WT older (black)
730 and KO older (grey). The traces were plotted by finding the difference between pre
731 and post blocker current trace for input step from -20mV to -80mV. Scale bar 100pA,
732 200msec.

733 (H) Line plot showing IV curve of XE 991 sensitive M current. There is no significant
734 difference in the M currents between WT older (filled black circles) and KO older
735 (grey diamond) for any of the input steps. (n=19 cells for both WT and KO, $F_{(1, 258)}$ =
736 2.54, p=0.11 between WT and KO, two-way ANOVA, error bars represent SEM)

737

738

739

740 **SK currents are elevated in older KO animals as compared to WT**

741

742 SK currents are also known to contribute substantially to mAHP (Sah and
743 Clements, 1999, Stocker et. al 1999). It has also been shown that Ca2+ influx from
744 VGCCs is elevated in FXS cells (Deng et al., 2011, 2013), indicating elevated Ca2+
745 levels intracellularly and hence increased SK channel activation. Thus, we
746 hypothesized that SK currents are elevated in FXS cells, leading to the observed
747 elevated mAHP in these cells. To test this, we used a procedure from Carlen, 1997.
748 Outward currents were evoked using step depolarization of the cell from -55mV to
749 +5mV and above (Fig 6A and 6B), in voltage clamp mode. Apamin was bath applied
750 to obtain post apamin trace. The difference current of pre apamin and post apamin
751 was quantified as SK currents. These currents were significantly higher in KO

752 animals as compared to WT for adult age group (SK current for older WT at +15mV
753 step 54.2 ± 9, n=13 cells; SK current for older KO at +15 mV step 131.73 ± 25.5,
754 n=13 cells; $F_{(1, 240)} = 33.3$, $p<0.001$ between WT and KO, two-way ANOVA)(Fig 6C).
755 However, this phenotype was only seen in adult WT vs adult KO animals. When
756 similar experiments were done in juveniles of both genotype, there was no significant
757 difference in SK currents (SK current for younger WT at +15mV step 61.93 ± 11.9,
758 n= 11 cells; SK current for younger KO at +15mV step 51.2 ± 8.9, n=9 cells; $F_{(1, 189)} =$
759 0.51, p=0.5, two way ANOVA) (Fig 6D). To delineate the developmental change in
760 SK channels levels between WT and KO, comparisons were made within the same
761 genotype, between different age groups. There was no significant change in the
762 levels of SK currents with age for WT animals (SK current for Older WT at +15mV
763 step 54.2 ± 9, n=13 cells; SK current for younger WT at +15mV step 61.93 ± 11.9, n=
764 11 cells; $F_{(1, 229)} = 0.01$, p=0.9 two way ANOVA) (Fig 6E). On the contrary there was
765 a significant increment in levels of SK currents for KO animals as they progressed
766 from juvenile to adult stage (SK current for older KO at +15 mV step 131.73 ± 25.5,
767 n=13 cells; SK current for younger KO at +15mV step 51.2 ± 8.9, n=9 cells;
768 $F_{(1,209)}=21.02$, $p<0.001$; two-way ANOVA) (Fig 6F). Together, these observations
769 show that there is an increase in levels of SK currents with age in KO animals, and
770 we note that this correlates with the worsening of spike reliability between adult and
771 juvenile KO animals as described in Fig 3.

772

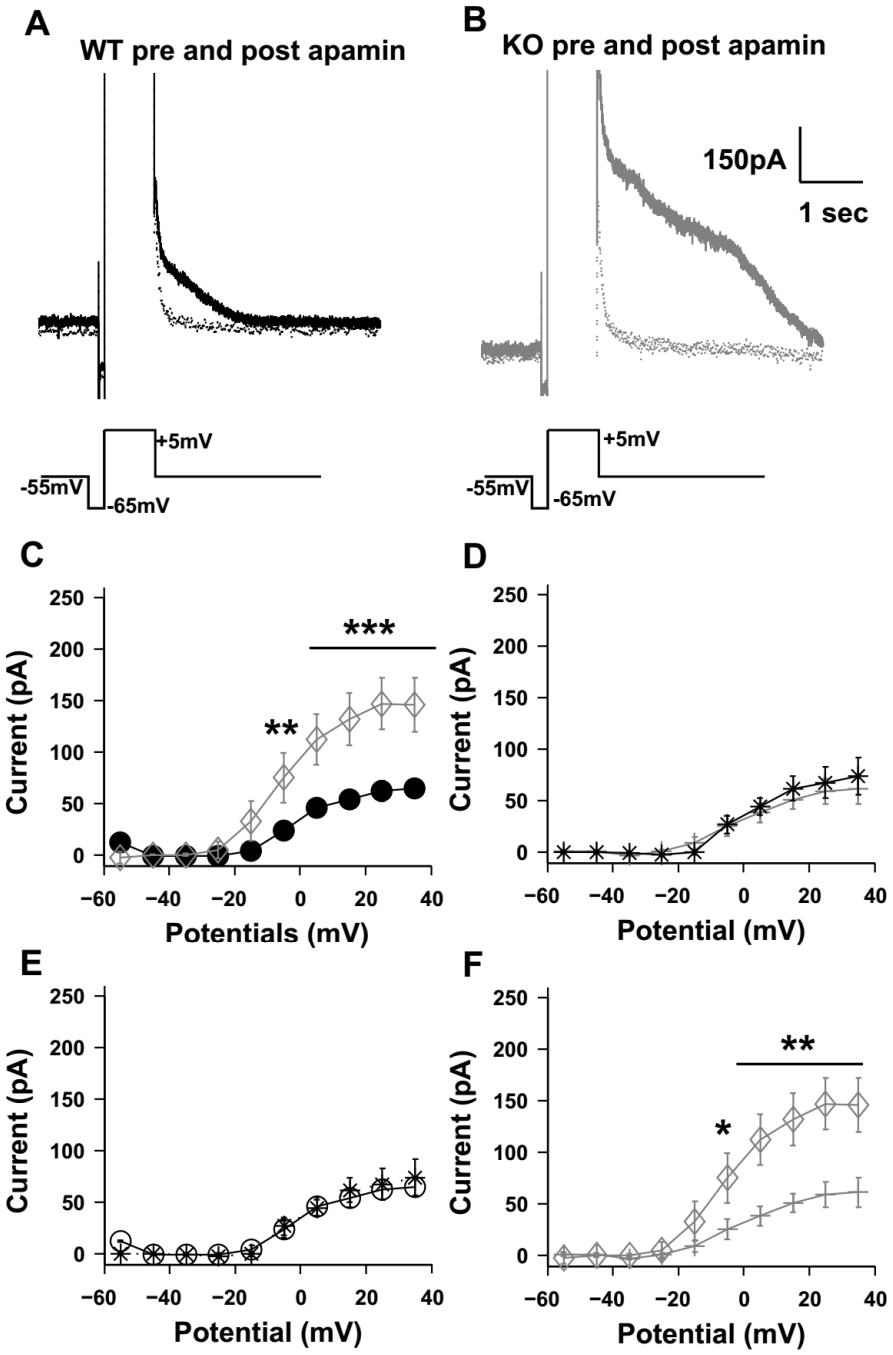

773

774 **Figure 6. Apamin sensitive SK currents are elevated in KO neurons as**

775 **compared to WT.**

776 (A) Representative traces showing the outward currents elicited by step

777 depolarization voltage commands in Voltage Clamp, for WT neuron (black) and (B)

778 for KO neuron (grey), pre apamin (solid line) and post apamin (dotted line) perfusion.
779 Trace below indicates command voltage protocol. Scale bar 150pA, 1sec.

780 (C) IV curve of the apamin sensitive current elicited across multiple steps for WT
781 older cells (n=13 cells, filled black circles) and KO older cells (n=13 cells, grey
782 diamond). Currents are significantly elevated for KO cells as compared to WT cells,
783 for multiple steps. ($F_{(1, 240)} = 33.3$, $p<0.001$ between WT and KO, two-way ANOVA,
784 error bars represent SEM)

785 (D) IV curve of the apamin sensitive current elicited across multiple steps WT
786 younger cells (n=11 cells, black star) and KO younger cells (n=9 cells, grey plus).
787 Currents between KO and WT cells at this age group were not significantly different.
788 ($F_{(1, 189)} = 0.51$; $p=0.5$; two way ANOVA, error bars represent SEM).

789 (E) IV curve of the apamin sensitive current elicited across multiple steps for WT
790 younger cells (n=11 cells, black stars) and WT older cells (n=13 cells, black circles).
791 There is no age dependent change in SK currents for WT animals ($F_{(1, 229)} = 0.01$,
792 $p=0.9$ two way ANOVA,error bars represent SEM).

793 (F) IV curve of the apamin sensitive current elicited across multiple steps for KO
794 younger cells (n=9 cells, grey plus) and KO older cells (n=13 cells, grey diamonds).
795 There is an age dependent increase in SK currents in KO animals ($F_{(1, 209)} = 21.02$,
796 $p<0.001$; two-way ANOVA, bars represent SEM).

797

798 **SK channel expression is unchanged in CA1 and CA3 regions for KO as**
799 **compared to WT**

800 We have observed that SK current levels are elevated in KO CA1 cells as
801 compared to WT (Fig 6). This elevation might arise due to increase in the levels of
802 SK channels or due to change in SK channel kinetics. The latter might arise due to
803 change in the kinetics of the SK channel itself or due to changes in activity of other
804 channels which have an effect on SK channels. The putative candidates might be
805 Ca^{2+} channels known to be effected in FXS (Meredith et al., 2007; Ferron et al.,
806 2014,Brown et al., 2001; Contractor et al., 2015). Previous published results have
807 not shown SK channels to be targets of FMRP for transcription regulation,
808 decreasing the likelihood that the levels will be affected in the CA1 region (Darnell et
809 al., 2011; Deng et al., 2018). To specifically test this point, immunofluorescence
810 experiments were used to assess the expression of SK channels. We performed in-
811 situ immunolabeling to measure the intensity of the SK2 isoform in CA3 and CA1
812 regions of the hippocampus using a specific antibody (Methods) (Fig 7A). We
813 analyzed levels of SK2 protein in different regions and sub sections of the
814 hippocampus for both WT and KO. Similar experiments were done on both adult and
815 juvenile slices. In juvenile animals, we have seen increased number of spikes in CA3
816 with no significant change in CA1 (Fig 4). However, the levels of SK2 protein were
817 not significantly altered in KO slices for either CA3 (N=4 animals for WT; N=4
818 animals for KO; $F_{(1, 24)} = 0.48$; p=0.5 for WT vs KO for CA3; two way ANOVA) (Fig
819 7B) or CA1 (N=4 animals for WT; N=4 animals for KO; $F_{(1, 24)} = 0.21$; p=0.6 for WT
820 vs KO for CA1; two way ANOVA) (7C). For adult animals we have seen reduction in
821 spike number in CA1 region (Fig 3G and 3H), but no changes in SK2 levels could be
822 found in either CA1 or CA3 (CA1: N=4 animals for WT; N=4 animals for KO; $F_{(1, 24)} =$
823 0.25; p = 0.61 for WT vs KO for CA1; two way ANOVA) (Fig 7E) (CA3: N=4 animals
824 for WT; N=4 animals for KO; $F_{(1, 24)} = 0.3$; p=0.6 for WT vs KO for CA3; two way

825 ANOVA) (Fig 7D). Overall, these labeling studies suggest that the KO does not affect
826 SK expression in either CA1 or CA3. The latter observation is in agreement with
827 previous results (Deng et al., 2018).

828

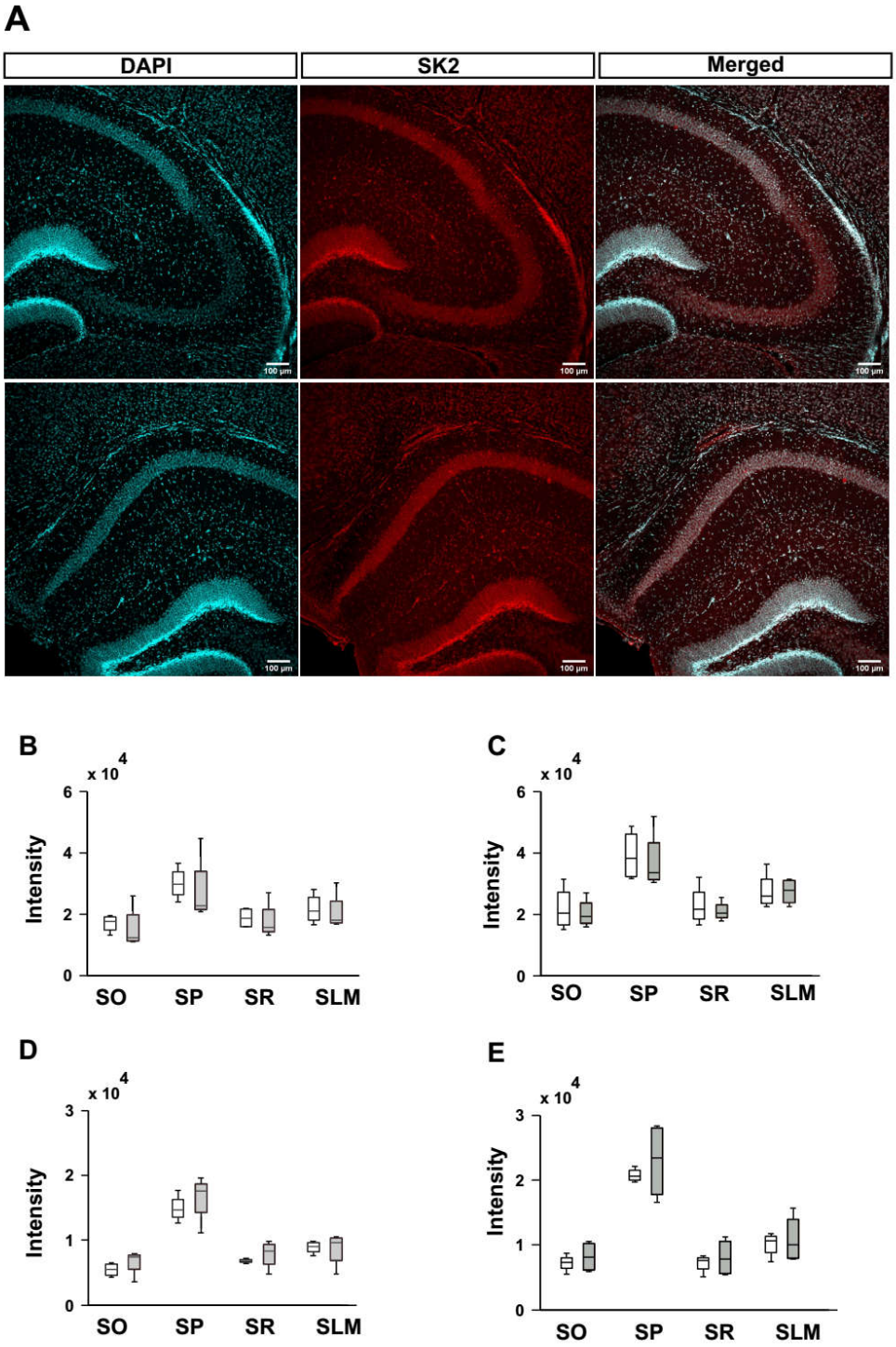

829

830 **Figure 7. There is no significant change in SK2 channel levels in KO as**
831 **compared to WT**

832 A. Representative images of SK2 labeling in CA3 (upper panel) and CA1 (lower
833 panel) for a WT animal. Green false color used for DAPI for better visualization.
834 Scale bar 100μm.

835 B. Analyzed box plot for mean intensity of SK2 channel in CA3 for juvenile
836 animals. (N=4 animals for WT; N=4 animals for KO; $F_{(1, 24)} = 0.48$; p=0.5
837 between WT and KO; two way ANOVA, error bars represent SEM)

838 C. Analyzed box plot for mean intensity of SK2 channel in CA1 for juvenile
839 animals. (N=4 animals for WT; N=4 animals for KO; $F_{(1, 24)} = 0.21$; p=0.6
840 between WT and KO for CA1; two way ANOVA, error bars represent SEM)

841 D. Analyzed box plot for mean intensity of SK2 channel in CA3 for adult animals.
842 (N=4 animals for WT; N=4 animals for KO; $F_{(1, 24)} = 0.3$; p=0.6 between WT and
843 KO for CA1, error bars represent SEM)

844 E. Analyzed box plot for mean intensity of SK2 channel in CA1 for adult animals.
845 (N=4 animals for WT; N=4 animals for KO; $F_{(1, 24)} = 0.25$; p=0.61 between WT
846 and KO for CA1; two way ANOVA, error bars represent SEM)

847

848 **Apamin partially rescues the phenotype of increased variability in KO animals**

849

850 Having shown that elevated and variable SK currents play a role in cellular
851 firing variability, we then asked if blockage of the SK current might rescue the
852 phenotype of increased variability. We observed that WT and KO populations

853 responded differently upon blocking SK currents using apamin. In WT cells, the
854 mean of within cell variability (CV_w) between trials increased (CV_w for WT cells pre
855 apamin 0.03 ± 0.002, n=13 cells; CV_w for WT cells post apamin 0.04 ± 0.005, n=13
856 cells) (Fig 8A,8B and 8E). However, for KO cells mean of within cell variability (CV_w)
857 between trials decreased (CV_w for KO cells pre apamin 0.06 ± 0.008, n=13 cells; CV_w
858 for KO cells post apamin 0.05 ± 0.009, n=13 cells) (Fig 8C,8D and 8E). Apamin
859 treatment had no significant affect on within-cell variability (CV_w) for either WT or KO.
860 However, it leads to a partial rescue such that post apamin KO CV_w values were not
861 significantly different from pre apamin WT CV_w values. A complete rescue by apamin
862 would have resulted in a significant reduction of the CV_w of KO cells (which did not
863 happen) as well as a convergence of variability between KO and WT (which did) ($F_{(1, 48)} = 0.96$
864 for effect of apamin; $F_{(1, 48)} = 0.004$ for WT and KO differences; two-way
865 ANOVA) (Fig 8E). We performed similar analysis for between cell (CV_b) variability.
866 Apamin perfusion led to a partial rescue in CV_b parameter as well such that there
867 was a significant reduction in CV_b of KO cells upon apamin perfusion, but no
868 convergence of variability between WT and KO (CV_b for WT cells pre apamin 0.414
869 ± 0.002; CV_b for WT cells post apamin 0.413 ± 0.002; CV_b for KO cells pre apamin
870 0.47 ± 0.003; CV_b for KO cells post apamin 0.43 ± 0.002; $F_{(1, 96)} = 157.5$; $p<0.001$ for
871 WT and KO differences; $F_{(1, 96)} = 53.1$; $p<0.001$ for effect of apamin on CV_b; two-way
872 ANOVA)(Fig 8F). CV_{s500} also showed a partial rescue with apamin perfusion (CV_{s500}
873 for WT cells pre apamin 0.042 ± 0.007; CV_{s500} for WT cells post apamin 0.042 ±
874 0.005; CV_{s500} for KO pre apamin 0.09 ± 0.03; CV_{s500} for KO post apamin 0.04 ±
875 0.007; $F_{(1, 49)} = 9.63$; $p=0.003$ for WT and KO differences; $F_{(1, 49)} = 2.87$; $p=0.09$ for
876 effect of apamin; two-way ANOVA) (Fig 8G). Overall, we find that blockage of SK

877 currents by apamin partially rescues the variability phenotypes, consistent with our
878 interpretation that elevation in SK currents has a role in variability.

879 **Blocking Calcium has no rescue affect**

880 From the above observations, blocking SK currents led to only a partial rescue in the
881 phenotype of increased imprecision and unreliability for spikes in KO cells. We
882 therefore asked if Ca^{2+}, as an upstream modulator of SK, could also contribute to a
883 partial rescue. To do this we used BAPTA to chelate intracellular Ca^{2+}. We added
884 BAPTA (10mM) into the intracellular recording pipette and assessed spike precision
885 10 minutes after patching. We found that chelating calcium using BAPTA led to
886 further increase in spike variability instead of rescue. Spike reliability within cell was
887 measured (CV_w) in these experiments and it was found that spikes became
888 significantly more variable post BAPTA than pre BAPTA for both WT and FXS cells
889 (CV_w for WT cells without BAPTA 0.038 ± 0.005, n=30 cells; CV_w for WT cells with
890 BAPTA 0.12 ± 0.02, n=12 cells; $p<0.001$; CV_w for KO cells without BAPTA 0.057 ±
891 0.006, n=29 cells; CV_w for KO cells with BAPTA 0.16 ± 0.04; $F_{(1, 81)} = 40.5$ $p<0.001$
892 for affect of BAPTA; two way ANOVA) (Fig 8H). Since Ca^{2+} has a large number of
893 ion-channels as other targets, we concluded that it was not a good target for rescue
894 of the variability phenotype.

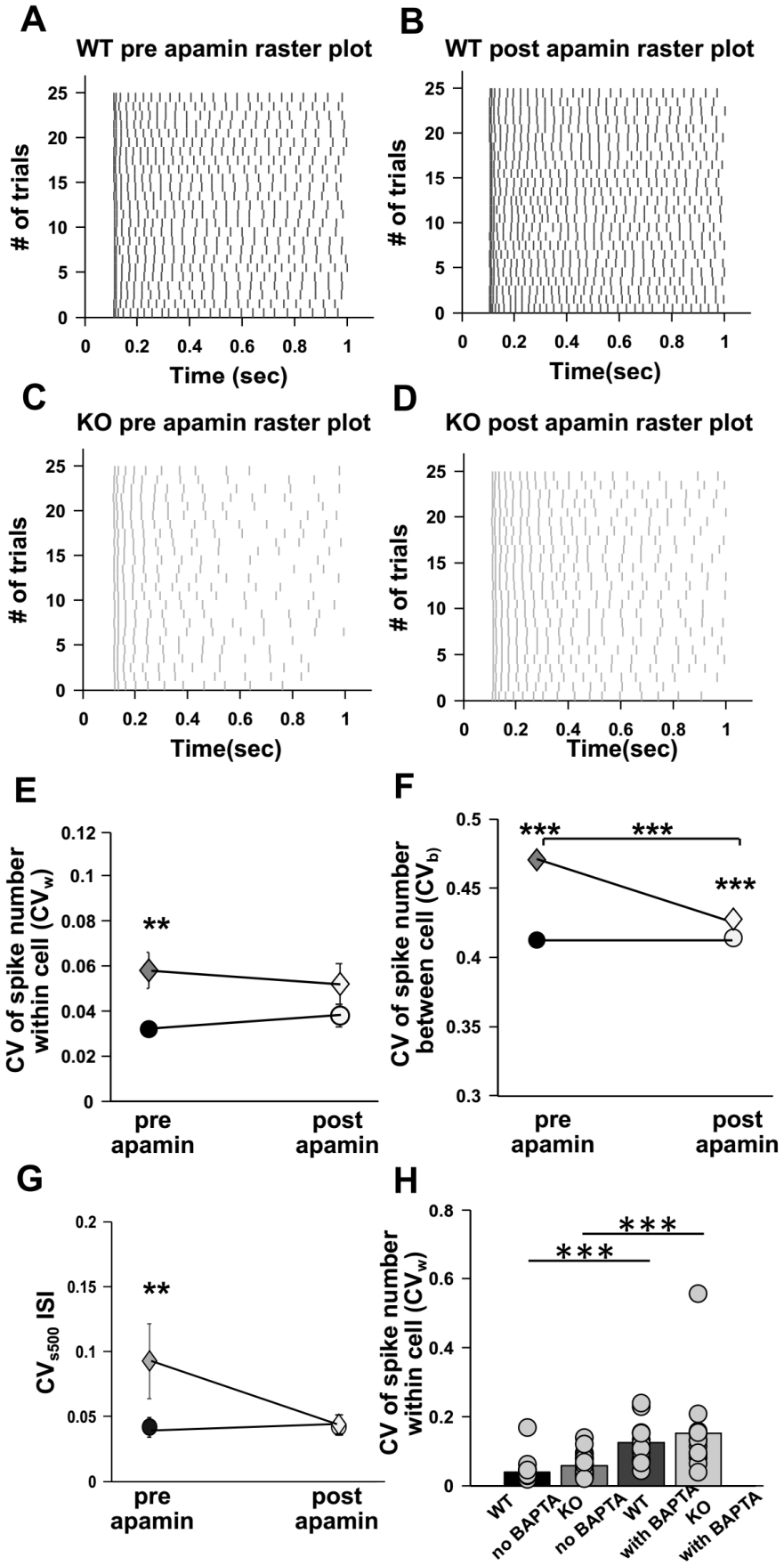
A
WT pre apamin raster plot
# of trials
Time (sec)
B
WT post apamin raster plot
# of trials
Time(sec)
C
KO pre apamin raster plot
# of trials
Time(sec)
D
KO post apamin raster plot
# of trials
Time(sec)
E
CV of spike number within cell (CVw)
**
pre apamin
post apamin
F
CV of spike number between cell (CVb)
***
***
***
pre apamin
post apamin
G
CVs500 ISI
**
pre apamin
post apamin
H
CV of spike number within cell (CVw)
***
***
WT no BAPTA
KO no BAPTA
WT with BAPTA
KO with BAPTA

895

896

897 **Figure 8 Partial rescue of within cell variability (CV_w) , between cell variability**
898 **(CV_b) and spike imprecision in KO neurons upon apamin perfusion.**

899 (A) Representative Raster plot showing spiking for step depolarization protocol for
900 WT, pre apamin.

901 (B) Representative Raster plot showing spiking for step depolarization protocol for
902 WT, post apamin. Same cell as A.

903 (C) Representative Raster plot showing spiking for step depolarization protocol for
904 KO, pre apamin.

905 (D) Representative Raster plot showing spiking for step depolarization protocol for
906 KO, post apamin. Same cell as C.

907 (E) Change in within cell variability parameter (CV_w) for pre (filled black circles) and
908 post apamin perfusion in WT (n=13 cells, empty black circles) and in KO (n=13 cells,
909 filled grey diamonds for pre apamin and empty grey diamonds for post apamin).
910 There is a partial rescue in CV_w parameter post apamin for KO cells vs. WT cells (F
911 $_{(1, 48)} = 0.96$ for effect of apamin; $F_{(1, 48)} = 0.004$ for WT and KO differences; 2-way
912 ANOVA with replication, error bars represent SEM)

913 (F) Plot showing change in between cell variability parameter (CV_b) for pre (filled
914 black circles) and post apamin perfusion WT (n=13 cells, empty black circles) and for
915 pre and post apamin perfusion KO (n=13 cells, filled grey diamonds for pre apamin
916 and empty grey diamonds for post apamin). There is a partial rescue in CV_b
917 parameter for KO cells vs. WT cells ($F_{(1, 96)} = 157.5$; $p<0.001$ for WT and KO

918 differences; $F_{(1, 96)} = 53.1$; $p<0.001$ for effect of apamin on $CV_{b;}$ two-way ANOVA with
919 replication error bars represent SEM).

920 (G) Plot for CV_{s500} for ISI, a measure of spike precision for pre (filled black circles)
921 and post apamin perfusion WT (n=13 cells, empty black circles) and for pre and post
922 apamin perfusion KO (n=13 cells, filled grey diamonds for pre apamin and empty
923 grey diamonds for post apamin). There is a partial rescue of CV_{s500} parameter upon
924 apamin perfusion ($F_{(1, 49)} = 9.63$; $p=0.003$ for WT and KO differences; $F_{(1, 49)} = 2.87$;
925 $p=0.09$ for effect of apamin; two-way ANOVA error bars represent SEM).

926 (H) Bar plot showing effect of BAPTA on within cell variability (CV_w) for WT (n=30
927 cells without BAPTA and n=12 cells with BAPTA) and KO (n=29 cells without BAPTA
928 and n=12 cells with BAPTA). Chelating Ca2+ using BAPTA, lead to a significant
929 increase in spike variability within cell (CV_w) for both WT and KO cells ($F_{(1, 81)} = 2.7$;
930 $p=0.1$ for differences between WT and KO; $F_{(1, 81)} = 40.5$ $p<0.001$ for affect of
931 BAPTA; 2-way ANOVA with replication, error bars represent SEM).

932

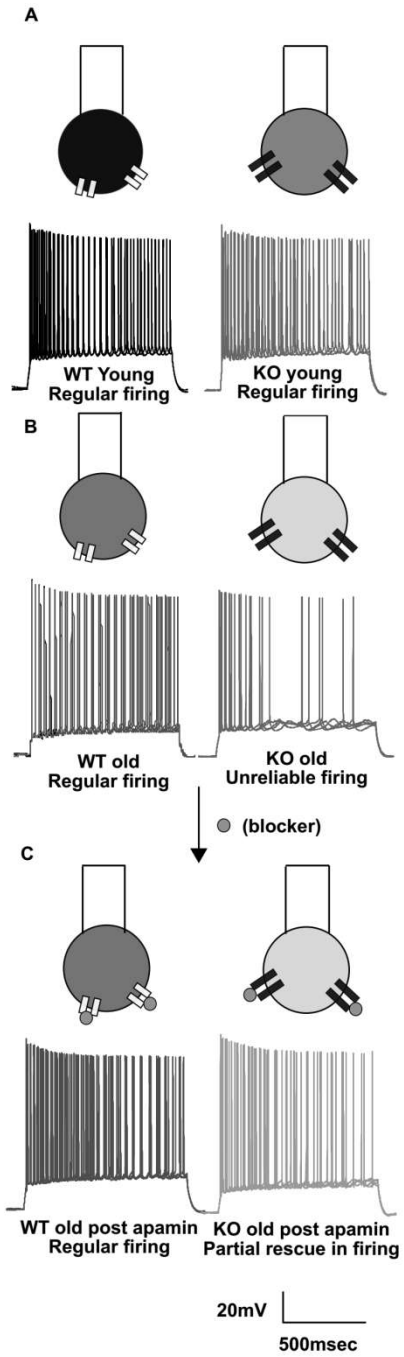

933

934 **Figure 9 Schematic summary plot indicating developmental increase in spiking**
935 **variability and the role of SK channels. All spiking traces are actual raw data**
936 **and show superimposed traces for 4 trials in WT (Black) and KO (Grey)**
937 **respectively.**

938 (A) Schematic of neurons, showing Younger WT (Black) and Younger KO (Grey). In
939 young animals we observe precise and reliable spiking across multiple trials. Scale
940 bar 20mV, 500msec.

941 (B) Schematic of Older WT and Older KO neurons. KO neurons have larger SK
942 currents which are represented by larger icons for SK channels. Noticeably, KO
943 spikes are more variable and less precise especially in the later part of the trial.

944 (C) Apamin (shown as small grey circles) is used to block SK channels present on
945 soma. Upon apamin perfusion spiking in WT (black) becomes more variable
946 whereas spiking in KO (light grey), increases in frequency leading to increased spike
947 precision and reliability.

948

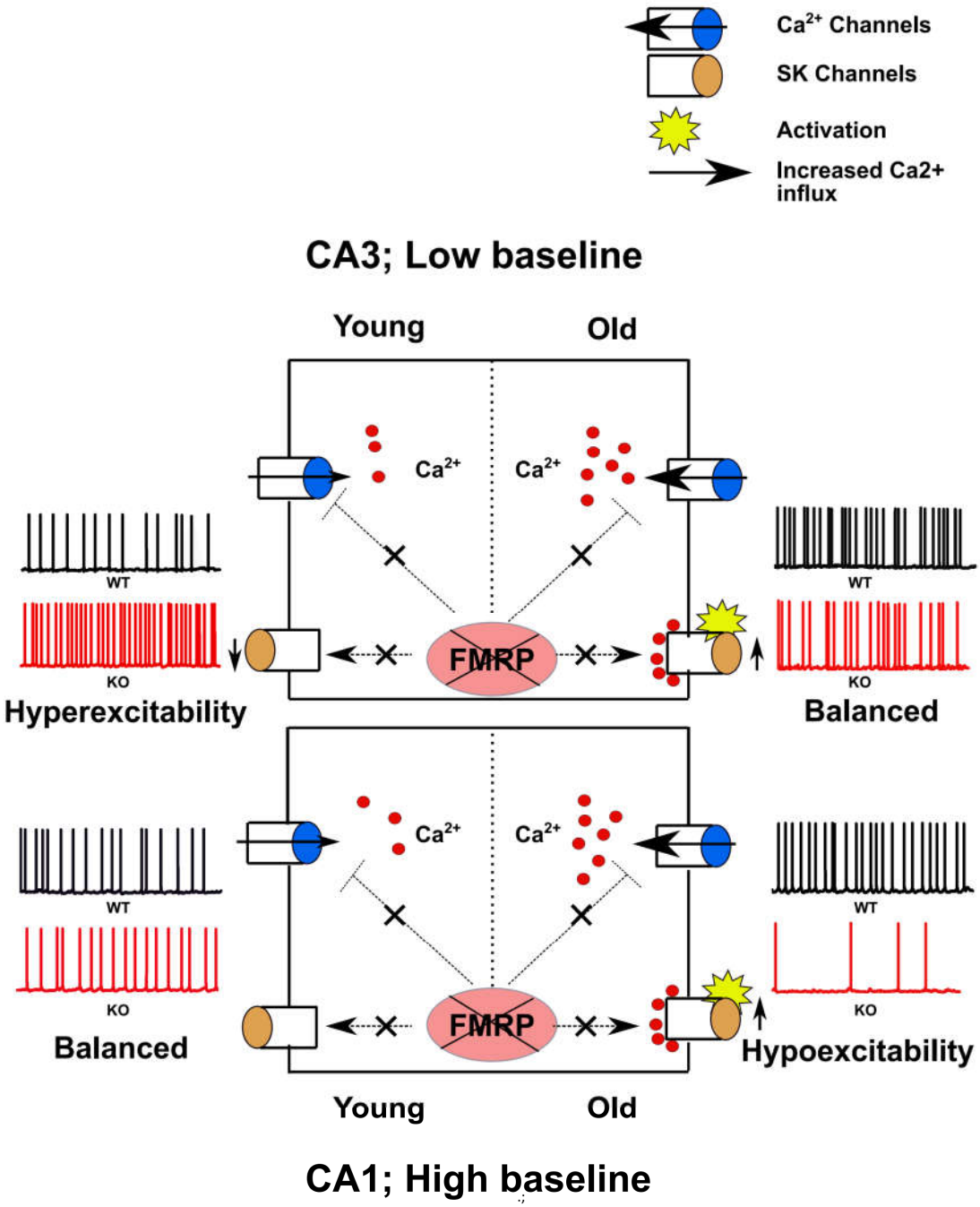

Figure 10. Schematic of a model explaining differential effect of FMRP KO in CA3 and CA1

(A) In young CA3 cells, loss of FMRP leads to reduced activation of SK channels which in turn gives neuronal hyperexcitability. However, as the animal matures

954 there is an increase in calcium influx in these cells. This compensates for this
955 reduced SK activity seen in young CA3 cells leading to a non significant change
956 in excitability for KO cells as compared to WT.

957 (B) In young CA1 cells, both WT and KO cells start with elevated excitability as a
958 result of which no significant differences can be seen between WT and KO.
959 However, as the animal matures, increase in Ca2+ influx brings excitability
960 down for both WT and KO. This decrease in excitability is significantly greater
961 for KO animals as many Ca2+ channels are known to be transcriptionally
962 regulated by FMRP. Under the absence of FMRP, these channels are known to
963 be elevated significantly making KO neurons hypoexcitable as compared to
964 WT.

965

966

967 **Table 1 - Summary of statistical tests**

Figure Number	Data structure	Type of test	Statistics
Fig 1E	Non normal	Wilcoxon rank sum test	p=0.0048 for CV_w differences between WT older and KO older.
Fig 1F	Non normal	Wilcoxon rank sum test	p<0.001 for CV_b differences between WT older and KO older.
Fig 1J	Non normal	2-way ANOVA	$F_{(1,113)}$ =5.78; p=0.018 for WT vs KO differences
Fig 2E	Normal	3-way ANOVA	p<0.001 for CV_w differences between WT older and KO older.
Fig 2F	Normal	3-way ANOVA	p<0.001 for CV_b differences between WT older and KO older.

Fig 3E	Normal	2-way ANOVA	$F_{(1,100)} = 4.97$; p=0.028 for WT and KO differences; $F_{(1,100)} = 8.05$; p=0.005 for interaction factor between age and genotype; p=0.7, for WT older vs WT younger; p<0.001 for KO older vs KO younger, ttest with bonferroni correction.
Fig 3F	Normal	2-way ANOVA	$F_{(1, 99)} = 7.47$, p=0.007 for age factor; $F_{(1,99)} = 9.46$; p=0.003 for interaction factor between age and genotype; p= 0.0002 for KO older vs KO younger; p=0.9 for WT older vs WT younger; p= 0.0025 for WT older and KO older
Fig 3G	Normal	2-way ANOVA	$F_{(1, 78)} = 5.1$; p=0.027 for spike number between WT and KO; p=0.029 between WT old and KO old; p=0.3 between WT young and KO young.
Fig 3J	Normal	2-way ANOVA	$F_{(1, 94)} = 0.03$; p=0.86 for WT and KO differences.
Fig 3K	Normal	2-way ANOVA	$F_{(1,923)} = 0.92$; p=0.33; WT and KO differences at young age group.
Fig 3L	Normal	2-way ANOVA	$F_{(1,1070)} = 31.03$ p<0.001; WT and KO differences at old age group
Fig 4B	Normal	2-way ANOVA	$F_{(1,72)} = 5.35$; p=0.023 for difference between WT and KO CA3 cells younger animals
Fig 4D	Normal	2-way ANOVA	$F_{(1,88)} = 1.06$; p=0.31 for difference between WT and KO CA1 cells younger animals
Fig 4F	Normal	2-way ANOVA	$F_{(1, 75)} = 1.16$; p=0.28 for difference between WT and KO CA3 cells older animals.
Fig 4H	Normal	2-way ANOVA	$F_{(1, 59)} = 7.42$; p=0.009 for difference between WT and KO CA1 cells for older animals.

Fig 5C	Normal	2-way ANOVA	$F_{(1, 46)} = 4.8$; p=0.033 for mAHP WT and KO differences. p=0.2 between WT younger and KO younger; p=0.017 for WT older and KO older.
Fig 5D	Normal	2-way ANOVA	$F_{(1, 54)} = 8.84$; p=0.004 for sAHP WT and KO differences. p=0.07 between WT younger and KO younger; p=0.008 for WT older and KO older.
Fig 5F	Non normal	Wilcoxon rank sum test	p=0.91 for I_h % sag between WT and KO
Fig 5H	Normal	2-way ANOVA	$F_{(1, 258)} = 2.54$; p=0.11 between WT and KO for I_M current
Fig 6C	Normal	2-way ANOVA	$F_{(1,240)} = 33.3$; p<0.001 for WT older and KO older SK currents
Fig 6D	Normal	2-way ANOVA	$F_{(1,189)} = 0.51$; p=0.5 for WT younger and KO younger SK currents
Fig 6E	Normal	2-way ANOVA	$F_{(1,229)} = 0.01$; p=0.9 for WT older and WT younger SK currents
Fig 6F	Normal	2-way ANOVA	$F_{(1,209)} = 21.02$; p<0.001 for KO older and KO younger SK currents
Fig 7B	Normal	2-way ANOVA	$F_{(1, 24)} = 0.48$; p=0.5 for WT younger vs KO younger for CA3
Fig 7C	Normal	2-way ANOVA	$F_{(1, 24)} = 0.21$; p=0.6 for WT younger vs KO younger for CA1
Fig 7D	Normal	2-way ANOVA	$F_{(1, 24)} = 0.3$; p=0.6 for WT older vs KO older for CA3
Fig 7E	Normal	2-way ANOVA	$F_{(1, 24)} = 0.25$; p=0.61 for WT older vs KO older for CA1
Fig 8E	Normal	2-way ANOVA	$F_{(1,48)} = 0.96$ for effect of apamin; $F_{(1,48)} = 0.004$ for WT and KO differences
Fig 8F	Normal	2-way ANOVA	$F_{(1,96)} = 157.5$; p<0.001 for WT and KO differences; $F_{(1,96)} = 53.1$; p<0.001 for effect of apamin on CV_b

Fig 8G	Normal	2-way ANOVA	$F_{(1, 49)} = 9.63$; p=0.003 for WT and KO differences; $F_{(1, 49)} = 2.87$; p=0.09 for effect of apamin; p=0.006 for WT pre apamin and KO pre apamin; p=0.05 for KO pre apamin and KO post apamin; p=0.23 WT pre apamin and KO post apamin.
Fig 8H	Normal	2-way ANOVA	$F_{(1, 81)} = 2.7$; p=0.1 for differences between WT and KO;$F_{(1, 81)} = .40.5$ p<0.001 for affect of BAPTA

Table 1 Detailed statistics used in different figures. It is to be noted that all of the data in figures is from CA1 cells except in figure 4, where it is from both CA3 and CA1 cells.

Discussion

We have used a mouse model of autism, the fragile X knockout mouse, to investigate cellular correlates of autism in hippocampal CA1 pyramidal neurons. We find that reliability of spiking is impaired in FXS adult animals. We observed an increase in spiking variability both within a cell over multiple trials and between cells

985 in matching trials, in FXS animals. The variability appeared between 6 and 8 weeks
986 of age, consistent with current understanding of autism as a neurodevelopmental
987 disorder. We observed that the increased spiking variability was accompanied by
988 reduced spiking and elevated mAHP currents. We further dissected out the channel
989 contributions to the elevated mAHP and found that SK currents were elevated in
990 adult FXS neurons. However, levels of SK channels were not different between WT
991 and KO mice. To test the hypothesis that elevated SK currents are responsible for
992 unreliable and imprecise spiking in FXS neurons, we used the specific SK blocker
993 apamin and obtained a partial rescue of the phenotype of increased spike variability.
994 In addition to this, we discovered a differential effect of FMRP KO in different
995 hippocampal regions. In agreement with previous published results, we found that
996 there is an increase in excitability in CA3 region of hippocampus, in juvenile animals.
997 At the same age, CA1 cells don't show any difference in excitability between WT and
998 KO. As the animal becomes older, we observe that the increased excitability seen in
999 CA3 goes away, and for CA1 cells in this age group there is an observation of
1000 reduced excitability. This is the first study which has shown that FMRP KO can lead
1001 to very different outcomes in different regions of the same brain structure, further
1002 highlighting the complexity of the disorder.

1003

1004 **Lowered spike reliability and spike imprecision at cellular intrinsic level in FXS**
1005 **KO hippocampal cells**

1006

1007 Our study demonstrates that there is a cell-intrinsic contribution to spiking variability
1008 in a mouse model of autism, and implicates increased currents from SK channels as

1009 part of the mechanism. This finding takes significance with the failure of mGluR
1010 antagonists and blockers to significantly alleviate FXS symptoms in human patients.
1011 These findings point to the likelihood that the mGluR theory (Erickson et al., 2017)
1012 may be incomplete. Specifically, our finding of within cell variability and between cell
1013 variability in FXS cells shows that cells in the mutant animals may form a
1014 heterogeneous population of intrinsically variable neurons, the combined effects of
1015 which may lead to network-level incoherence.

1016 This variability in neuronal responses over multiple trials may have implications for
1017 multiple behaviors. For example, in learning, the stimulus typically needs to be
1018 repeated over multiple trials. If the response of a cell at its intrinsic level as well as
1019 between cells is variable, the precision of input spiking as well as output activity
1020 would be reduced. This would adversely impact learning rules such as STDP and
1021 associativity (Markram et al., 1997; Bi and Poo, 1998). Further, elevated SK
1022 currents will have a direct impact on the recorded sEPSPs at the soma (Ngo-Anh et
1023 al., 2005).

1024

1025 **SK channel currents elevation may underlie previously observed age**
1026 **dependent changes in KO cellular physiology**

1027

1028 FXS has many clinical and experimental attributes of a neurodevelopmental
1029 syndrome (Nimchinsky et al., 2001; Cruz-Martin et al., 2010; Meredith et al., 2012).
1030 An age-dependent decline in learning has been shown in the drosophila Fragile X
1031 model (Choi et al., 2010). Theta Burst Stimulation (TBS) LTP has been showed to
1032 produced exaggerated LTP in anterior piriform cortex for older KO mice (12-18

1033 months) but not in younger mice (< 6mths)(Larson, 2005). Similar results were seen
1034 in Prefrontal Cortex where TBS produced a significant impairment in LTP for 12
1035 month old mice but not in 2 month old animals (Martin et al., 2016). Even in humans
1036 it has been shown that the males who have a premutation (have CGG repeats <200)
1037 predominantly demonstrated fragile-X associated tremor/ataxia syndrome (FXTAS)
1038 among patients who were over 50 years old (Cornish et al., 2008). At the molecular
1039 level, an age dependent change has also been shown in protein levels in FXS from
1040 P17 mice to adults (Tang et al., 2015)

1041 We observed a similar age dependent change in the spike variability phenotype,
1042 which was absent in young KO animals, but manifested in older (>6 week) mice
1043 (Figure 3E). Age dependent changes in SK channels have been previously reported
1044 such that the levels of SK channels are elevated in older animals as compared to
1045 younger ones (Blank et al., 2003). This complements our finding that the AHP
1046 difference between WT and KO animals arose in older animals (Fig 5) and that the
1047 SK channel underlay the difference in the older animals. There are also evidence of
1048 age related changes in Ca^{2+} levels and Ca^{2+} uptake mechanisms, such that basal
1049 Ca^{2+} levels are elevated in aging brains (Das and Ghosh, 1996; Kirischuk et al.,
1050 1996; Foster and Norris, 1997). Such altered Ca2+ levels would also have a direct
1051 impact on the functionality of SK channels. We were not able to directly investigate
1052 this possible upstream effect due to the very diverse outcomes of modulating
1053 calcium signaling (Figure 8H)

1054

1055

1056 **SK channels may be an FMRP target with multiple physiological and**
1057 **behavioral outcomes.**

1058

1059 FMRP targets multiple downstream pathways. It not only is a transcription factor but
1060 its N-terminus is known to interact with multiple other proteins affecting their
1061 functioning (Brown et al., 2010; Deng et al., 2013). Thus mutations in FMRP affect
1062 multiple aspects of cellular functioning. Previous RNA-seq results have not shown
1063 that SK channels are elevated or affected in FXS (Brown et al., 2001; Darnell et al.,
1064 2011). However, the functioning of SK currents might be subject to other indirect
1065 effects such as changes in Calcium channel distribution, or in their functioning
1066 (Meredith et al., 2007; Ferron et al., 2014). Alterations in SK channels have
1067 substantial implications for multiple other phenotypes at the cellular and behavioral
1068 level. Previous studies have found that FXS KOs have impaired LTP in CA1
1069 hippocampus (Lauterborn et al., 2007; Lee et al., 2012; Tian et al., 2017). We
1070 suggest that this impairment might be partially due to elevated SK currents, which
1071 are known to shunt EPSPs and also to increase NMDA Mg^{2+} block (Ngo-Anh et al.,
1072 2005). Hence our observation of elevated SK currents is consistent with the reported
1073 increase LTP threshold in FXS (Lee et al., 2012). These effects on LTP may have
1074 knock-on effects on memory phenotypes in FXS models. For example, a mild
1075 impairment in learning due to change in platform location in the Morris water maze
1076 test has been found in FXS models (D ’hooge et al., 1997; Dobkin et al., 2000).SK
1077 currents have been shown to be reduced after learning and this reduction leads
1078 decreased variability in spiking events (Sourdet et al., 2003).

1079 **Comparison with previously published studies**.

1080 Multiple previous studies have found hyper excitability in hippocampus in FXS model
1081 mice (Deng and Klyachko, 2016; Luque et al., 2017). We do not find a strong
1082 significant difference between KO and WT f-I curves (Fig 3I,3J, 3K and 3L).
1083 However, the previously published studies were carried out in the FVB strain of mice
1084 and the present study was done on BL/6. Strain dependent differences in FXS have
1085 previously been found (Paradee et al., 1999; Dobkin et al., 2000; Lee et al., 2012;
1086 Routh et al., 2013). However, (Brager et al., 2012) found a lowering of Input
1087 Resistance for KO CA1 cells indicative of reduced excitability. Telias et al 2015 have
1088 found similar phenotype as ours in human hippocampal culture cells. In their study,
1089 they found that FXS cells were incapable of producing multiple spikes on sustained
1090 depolarization at multiple holding potentials, similar to what we observe in this study.
1091 It is interesting to note that most excitability analyses and f-I curves use 500 ms
1092 current steps, whereas in our study a difference arises after 600 ms, and leads to a
1093 reduction in excitability in the KO (Figure 1B and 1I). This suggests that a nuanced
1094 interpretation of such excitability studies is desirable, as the responses may have
1095 complex temporal features not reducible to a single measure of excitability. Another
1096 important point of difference is the age of the animals. Previous published studies
1097 have been done on relatively young animals (<P30) as compared to the present
1098 study, where adult animals (6-8 wks) have also been used for the experiments. Our
1099 own results (Figure 4B and 4C) show that there is a substantial change in spiking
1100 variability as well as AHPs as the animal matures. Other studies have also reported
1101 an age-dependent effect of expression of plasticity phenotypes in FXS mice (Larson,
1102 2005; Martin et al., 2016). Fragile X Syndrome is known to be a developmental
1103 disease where symptoms and many other biochemical and other pathways are
1104 known to undergo changes with the age of the animal. Hence it may be important to

1105 factor in age-dependence and possibly use a wider range of ages to re-examine
1106 some of the conclusions that have been made from FXS models.

1107 Our study is also the first to examine the effect of variability and spiking asynchrony,
1108 which again we find to be an age-dependent effect. We postulate that variability in
1109 firing of individual cells, which previous studies have not explicitly examined, may be
1110 a further complicating factor in analyzing baseline changes arising due to the FMRP
1111 mutation.

1112

1113 **FMRP KO has different physiological outcomes in different regions of the**
1114 **hippocampus brain regions**

1115 In the present study, we make the important and unexpected finding that
1116 FMRP KO has differential cell-physiological effects on different sub sections of the
1117 same brain region. In an attempt to replicate previous results, we found that there is
1118 hyperexcitability in pyramidal neurons of the CA3 region in juvenile mice (as
1119 previously reported by Deng et al 2019) but there was no significant difference in
1120 spiking in the CA1 region at the same age. Further, the phenotype reverses for CA1
1121 cells in adult FMRP KO animals such that pyramidal neurons have reduced
1122 excitability, whereas for CA3 regions the hyperexcitability goes away. We suggest
1123 that these differential effects arise from the balance of effects between the direct
1124 effects of FMRP on SK channels, the indirect effects of FMRP on SK via calcium,
1125 and the effects of age, again potentially via calcium.

1126 Direct effects of FMRP on SK: Deng et. al. 2019 has shown that absence of FMRP
1127 leads to reduced activity of SK channels. They have shown that a physical
1128 interaction between FMRP and SK, leads to activation of SK channels. This

1129 suggests that FMRP is a direct activator of SK channels. In the case of mutant
1130 animals where FMRP is absent, there is a reduction in SK currents leading to
1131 hyperexcitability which has been observed both in the present and previous study.
1132 (Fig 10A). We see this effect in CA3 cells for KO animals at younger age group.

1133 Indirect effects on SK via calcium: SK channels are dependent on intracellular
1134 calcium for their activation. Calcium channels are known targets of FMRP for
1135 transcription regulators(Brown et al., 2001; Darnell et al., 2011). Calcium influx via L
1136 type Ca2+ channels are known to be elevated in Neural Progenitor Cells (NPCs)
1137 (Danesi et al., 2018). Cortical culture neurons have been shown to have significantly
1138 elevated basal calcium levels in FXS neuron (Castagnola et al., 2018) and there is
1139 increased calcium influx in CA3 cells (Deng et al., 2011, 2013). In reference to
1140 human patients, multiple point mutations in Ca^{2+} genes are associated with autism
1141 (Contractor et al., 2015; Pinggera et al., 2015; Nguyen et al., 2018). There are
1142 multiple other studies in other neuron types which show increased intracellular
1143 calcium in autism models(Laumonnier et al., 2006; Krey and Dolmetsch, 2007;
1144 Tessier and Broadie, 2011; Pinggera et al., 2015; Limpitikul et al., 2016). These
1145 studies are in agreement with our observations in the present study where we see
1146 increased SK currents in CA1 cells, which is expected if the intracellular calcium
1147 levels are elevated in FXS neurons. (Fig 10A). This increased calcium influx can
1148 explain the reduced excitability phenotypes seen in older CA3 and CA1 cells.

1149 Effects of age on calcium: Calcium binding proteins and intracellular calcium
1150 dynamics are known to undergo development dependent alterations in FXS neurons
1151 (Tessier and Broadie, 2011). Calcium levels and Ca2+ uptake mechanisms, are also
1152 known to undergo changes with aging in animals (Das and Ghosh, 1996; Kirischuk
1153 et al., 1996; Foster and Norris, 1997). Though there are limited studies available in

1154 reference to change in calcium channel levels with age in autism models, we
1155 hypothesize that a change in calcium dynamics is consistent with the fact that autism
1156 is a neurodevelopment disorder. (Fig 10A and 10B). We see this effect in both CA3
1157 and CA1 regions for KO animal, where in CA3 increased excitability seen in younger
1158 animal levels off as the animal becomes adult. On the other hand, because of the
1159 increase in calcium, CA1 cells in which excitability was balanced at young age group
1160 goes in the direction of hypoexcitability at older age groups.

1161 Based on these findings, we propose a schematic model to explain these
1162 differences (Fig 10). In young age group for KO CA3 cells, absence of FMRP leads
1163 to hyperexcitability as explained above. As the animal becomes older this effect goes
1164 away due to increased calcium influx with age leading to SK activation and balancing
1165 out hyperexcitability (Fig 10A). On the other hand for young KO CA1 cells, both WT
1166 and KO start with maximum increased excitability where it is not significantly
1167 different. As the animal becomes older, increased calcium influx moves KO cells
1168 towards hypoexcitability (Fig 10B)

1169 **Defects in single cell physiology may lead to network and population**
1170 **asynchrony**

1171 Multiple studies have shown that variability or lack of coordination in spiking exists
1172 in FXS at the network level (Arbab et al., 2018; Talbot et al., 2018). In these tetrode-
1173 based studies, variability has been shown at the level of cellular firing patterns in the
1174 in-vivo network, hence it is difficult to separate cell-intrinsic properties from synaptic
1175 and network phenomena. In our study, we use the CV_b parameter to gain an
1176 understanding about the correlation between cells at a population level. Using this
1177 analysis we have tried to estimate the variability which exists between individual

1178 neurons responses when actually neurons were recorded one at a time. In contrast
1179 to tetrode recordings or field response recordings, where the recorded response is a
1180 resultant of multiple neurons and hence is a population response, CV_b remains an
1181 intrinsic response of neurons depending on its active channels. CV_b is an indirect
1182 readout of network correlations and should not be inferred as giving actual network
1183 correlation information. Clear mechanisms are lacking for this reported asynchrony.
1184 However, prior researchers have postulated that synaptic mechanisms may be
1185 responsible for the observed asynchrony (Talbot et al., 2018). Our study provides an
1186 alternative hypothesis for the mechanism, namely, that the effect is cell-intrinsic and
1187 is in part due to altered kinetics of SK channels. Other studies provide evidence in
1188 favor of a role for SK channels in mediating precision and synchronous firing. For
1189 example, (Deister et al., 2009), showed that SK channels were responsible for
1190 mediating precision in autonomous firing in Globus Pallidus neurons. (Schultheiss et
1191 al., 2010) showed that dendritic SK channels also control synchronization. Another
1192 study by (Kleiman-Weiner et al., 2009) has shown that SK channels play a role in
1193 mediating thalamocortical oscillations. A study by (Combe et al., 2018) shows that
1194 SK channels contribute to phase locking for spiking of CA1 cells of the hippocampus
1195 to slow gamma frequency inputs from Schaffer Collaterals (SC). Thus, alterations in
1196 SK channel kinetics in FXS mutants as established by our study might have
1197 substantial impacts on phase coding and synchronization of hippocampal cell
1198 populations.

1199

1200 **A theory of FXS pathophysiology**

1201 An alternate theory to mGLUR theory in explanation of FXS pathophysiology is the
1202 'discoordination' theory. The idea behind this theory, is that many of the cognitive
1203 impairments seen in FXS are due to altered coordination in spiking of cells in
1204 networks, which might be either due to an imbalance in excitation-inhibition in the
1205 networks (El Idrissi et al., 2005; Heulens et al., 2012) or due to an intrinsic
1206 incoherent tendency of the neurons (Brock et al., 2002; Fenton, 2015; Radwan et al.,
1207 2016). Though this theory is preliminary, it may offer a promising alternative point of
1208 view from the tranditional mGLUR theory. Some studies have shown that intrinsic
1209 changes in cells during FXS effect their E/I balance (Zhang et al., 2014; Lee et al.,
1210 2017) and modulation of these channels lead to rescue of FXS phenotype This
1211 present study has probed dysfunction of a specific ion channel, SK which was shown
1212 to effect the spiking variability at single cell level. It is an addition to the increasing list
1213 of ion channels which are known to be affected in FXS and may have an important
1214 effect on FXS etiology.

1215

1216

1217

1218

1219 **References**

1220

1221 Arbab T, Battaglia FP, Pennartz CMA, Bosman CA (2018) Abnormal hippocampal
1222 theta and gamma hypersynchrony produces network and spike timing
1223 disturbances in the Fmr1-KO mouse model of Fragile X syndrome. Neurobiol

1224 Dis 114:65–73
1225 Arbab T, Pennartz CMA, Battaglia FP (2018) Impaired hippocampal representation
1226 of place in the Fmr1-knockout mouse model of fragile X syndrome. Sci Rep.
1227 Bacci A, Huguenard JR (2006) Enhancement of spike-timing precision by autaptic
1228 transmission in neocortical inhibitory interneurons. Neuron.
1229 Bi G, Poo M (1998) Synaptic Modifications in Cultured Hippocampal Neurons :
1230 Dependence on Spike Timing , Synaptic Strength , and Postsynaptic Cell Type.
1231 18:10464–10472.
1232 Blank T, Nijholt I, Kye MJ, Radulovic J, Spiess J (2003) Small-conductance, Ca2+-
1233 activated K+channel SK3 generates age-related memory and LTP deficits. Nat
1234 Neurosci 6:911–912.
1235 Brager DH, Akhavan AR, Johnston D (2012) Impaired Dendritic Expression and
1236 Plasticity of h-Channels in the fmr1-/yMouse Model of Fragile X Syndrome. Cell
1237 Rep.
1238 Brock JON, Brown CC, Boucher J (2002) The temporal binding deficit hypothesis of
1239 autism. 14:209–224.
1240 Brown MR, Kronengold J, Gazula VR, Chen Y, Strumbos JG, Sigworth FJ,
1241 Navaratnam D, Kaczmarek LK (2010) Fragile X mental retardation protein
1242 controls gating of the sodium-activated potassium channel Slack. Nat Neurosci.
1243 Brown V, Jin P, Ceman S, Darnell JC, Donnell WTO, Tenenbaum SA, Jin X, Feng Y,
1244 Wilkinson KD, Keene JD, Darnell RB, Warren ST, Carolina N (2001a)
1245 Microarray Identification of FMRP-Associated Brain mRNAs and Altered mRNA
1246 Translational Profiles in Fragile X Syndrome. 107:477–487.
1247 Brown V, Jin P, Ceman S, Darnell JC, O'donnell WT, Tenenbaum SA, Jin X, Feng Y,
1248 Wilkinson KD, Keene JD, Darnell RB, Warren ST (2001b) Microarray

1249 Identification of FMRP-Associated Brain mRNAs and Altered mRNA
1250 Translational Profiles in Fragile X Syndrome Howard Hughes Medical Institute
1251 Department of Human Genetics FMRP is largely cytoplasmic, incorporated into
1252 large messenger-ribonucleopr. Available at:
1253 http://www.cell.com/cgi/content/full/107/4/.
1254 Carandini M (2004) Amplification of Trial-to-Trial Response Variability by Neurons in
1255 Visual Cortex. 2.
1256 Carlen PL (1997) Reversible inhibition of I K , I AHP , I h and I Ca currents by
1257 internally applied gluconate in rat hippocampal pyramidal neurones. :343–350.
1258 Castagnola S, Delhaye S, Folci A, Paquet A, Brau F, Duprat F, Jarjat M, Grossi M,
1259 Béal M (2018) New Insights Into the Role of Ca v 2 Protein Family in Calcium
1260 Flux Deregulation in Fmr1 -KO Neurons. 11:1–13.
1261 Choi CH, McBride SMJ, Schoenfeld BP, Liebelt DA, Ferreiro D, Ferrick NJ, Hinchey
1262 P, Kollaros M, Rudominer RL, Terlizzi AM, Koenigsberg E, Wang Y, Sumida A,
1263 Nguyen HT, Bell AJ, McDonald T V., Jongens TA (2010a) Age-dependent
1264 cognitive impairment in a Drosophila Fragile X model and its pharmacological
1265 rescue. Biogerontology.
1266 Choi CH, McBride SMJ, Schoenfeld BP, Liebelt DA, Ferreiro D, Ferrick NJ, Hinchey
1267 P, Kollaros M, Rudominer RL, Terlizzi AM, Koenigsberg E, Wang Y, Sumida A,
1268 Nguyen HT, Bell AJ, McDonald T V., Jongens TA (2010b) Age-dependent
1269 cognitive impairment in a Drosophila Fragile X model and its pharmacological
1270 rescue. Biogerontology 11:347–362.
1271 Combe CL, Canavier CC, Gasparini S (2018) Intrinsic mechanisms of frequency
1272 selectivity in the proximal dendrites of CA1 pyramidal neurons. J Neurosci
1273 38:0449–18 Available at:

http://www.jneurosci.org/lookup/doi/10.1523/JNEUROSCI.0449-18.2018.

Contractor A, Klyachko VA, Portera-Cailliau C (2015a) Altered Neuronal and Circuit Excitability in Fragile X Syndrome. Neuron.

Contractor A, Klyachko VA, Portera-Cailliau C (2015b) Altered Neuronal and Circuit Excitability in Fragile X Syndrome. Neuron 87:699–715 Available at: http://dx.doi.org/10.1016/j.neuron.2015.06.017.

Cornish KM, Li L, Kogan CS, Jacquemont S, Turk J, Dalton A, Hagerman RJ, Hagerman PJ (2008a) Age-dependent cognitive changes in carriers of the fragile X syndrome. Cortex 44:628–636.

Cornish KM, Li L, Kogan CS, Jacquemont S, Turk J, Dalton A, Hagerman RJ, Hagerman PJ (2008b) Age-dependent cognitive changes in carriers of the fragile X syndrome. Cortex.

Crook SM, Ermentrout GB, Bower JM (1998) Spike Frequency Adaptation Affects the Synchronization Properties of Networks of Cortical Oscillators. Neural Comput.

Cruz-Martin A, Crespo M, Portera-Cailliau C (2010) Delayed Stabilization of Dendritic Spines in Fragile X Mice. J Neurosci 30:7793–7803 Available at: http://www.jneurosci.org/cgi/doi/10.1523/JNEUROSCI.0577-10.2010.

Cudmore RH, Fronzaroli-Molinieres L, Giraud P, Debanne D (2010) Spike-Time Precision and Network Synchrony Are Controlled by the Homeostatic Regulation of the D-Type Potassium Current. J Neurosci 30:12885–12895 Available at: http://www.jneurosci.org/cgi/doi/10.1523/JNEUROSCI.0740-10.2010.

D ’hooge R, Nagels G, Franck F, Bakker CE, Reyniers # E, Storm K, Kooy RF, Oostra BA, Willems: PJ, De Deyn PP (1997) MILDLY IMPAIRED WATER MAZE PERFORMANCE IN MALE Fmrl KNOCKOUT MICE. ~ Pergamon Neurosci

1299 76:367–376.
1300 Danesi C, Achuta VS, Corcoran P, Peteri U, Turconi G (2018) Stem Cell Reports.
1301 11:1449–1461.
1302 Darnell JC, Driesche SJ Van, Zhang C, Ying K, Hung S, Mele A, Fraser CE, Stone
1303 EF, Chen C, Fak JJ, Chi SW, Licatalosi DD, Richter JD, Darnell RB (2011a)
1304 FMRP Stalls Ribosomal Translocation on mRNAs Linked to Synaptic Function
1305 and Autism. Cell 146:247–261 Available at:
1306 http://dx.doi.org/10.1016/j.cell.2011.06.013.
1307 Darnell JC, Van Driesche SJ, Zhang C, Hung KYS, Mele A, Fraser CE, Stone EF,
1308 Chen C, Fak JJ, Chi SW, Licatalosi DD, Richter JD, Darnell RB (2011b) FMRP
1309 stalls ribosomal translocation on mRNAs linked to synaptic function and autism.
1310 Cell.
1311 Das N, Ghosh S (1996) The effect of age on calcium dynamics in rat brain in vivo.
1312 Mech Ageing Dev.
1313 Deister CA, Chan CS, Surmeier DJ, Wilson CJ (2009) Calcium-Activated SK
1314 Channels Influence Voltage-Gated Ion Channels to Determine the Precision of
1315 Firing in Globus Pallidus Neurons. J Neurosci.
1316 Deng P-Y, Sojka D, Klyachko VA (2011) Abnormal Presynaptic Short-Term Plasticity
1317 and Information Processing in a Mouse Model of Fragile X Syndrome. J
1318 Neurosci.
1319 Deng P, Carlin D, Oh YM, Myrick LK, Warren ST, Cavalli V, Klyachko VA (2018)
1320 Voltage-Independent SK Channel Dysfunction Causes Neuronal
1321 Hyperexcitability in the Hippocampus of Fmr1 KO mice Voltage-Independent SK
1322 Channel Dysfunction Causes Neuronal Hyperexcitability in the Hippocampus of
1323 Fmr1 KO mice Abbreviated Title : SK Channel .

1324 Deng PY, Klyachko VA (2016) Increased Persistent Sodium Current Causes
1325 Neuronal Hyperexcitability in the Entorhinal Cortex of Fmr1 Knockout Mice. Cell
1326 Rep.
1327 Deng PY, Rotman Z, Blundon JA, Cho Y, Cui J, Cavalli V, Zakharenko SS, Klyachko
1328 VA (2013) FMRP Regulates Neurotransmitter Release and Synaptic Information
1329 Transmission by Modulating Action Potential Duration via BK Channels. Neuron.
1330 Dobkin C, Rabe A, Dumas R, El Idrissi A, Haubenstock H, Ted Brown W (2000)
1331 Fmr1 knockout mouse has a distinctive strain-specific learning impairment.
1332 Neuroscience.
1333 El Idrissi A, Ding XH, Scalia J, Trenkner E, Brown WT, Dobkin C (2005) Decreased
1334 GABAA receptor expression in the seizure-prone fragile X mouse. Neurosci Lett
1335 377:141–146.
1336 Erickson CA, Davenport MH, Schaefer TL, Wink LK, Pedapati E V., Sweeney JA,
1337 Fitzpatrick SE, Brown WT, Budimirovic D, Hagerman RJ, Hessl D, Kaufmann
1338 WE, Berry-Kravis E (2017) Fragile X targeted pharmacotherapy: Lessons
1339 learned and future directions. J Neurodev Disord 9:1–14.
1340 Faisal AA, Selen LPJ, Wolpert DM (2008) Noise in the nervous system. Nat Rev
1341 Neurosci.
1342 Ferron L, Nieto-Rostro M, Cassidy JS, Dolphin AC (2014a) Fragile X mental
1343 retardation protein controls synaptic vesicle exocytosis by modulating N-type
1344 calcium channel density. Nat Commun.
1345 Ferron L, Nieto-Rostro M, Cassidy JS, Dolphin AC (2014b) Fragile X mental
1346 retardation protein controls synaptic vesicle exocytosis by modulating N-type
1347 calcium channel density. Nat Commun 5:1–14 Available at:
1348 http://dx.doi.org/10.1038/ncomms4628.

1349 Foster TC, Norris CM (1997) Age-associated changes in ca2+-dependent processes:
1350 Relation to hippocampal synaptic plasticity. Hippocampus.
1351 Fricker D, Miles R (2000) EPSP amplification and the precision of spike timing in
1352 hippocampal neurons. Neuron.
1353 Fujisawa S, Yamada MK, Nishiyama N, Matsuki N, Ikegaya Y (2004) BDNF boosts
1354 spike fidelity in chaotic neural oscillations. Biophys J 86:1820–1828 Available at:
1355 http://dx.doi.org/10.1016/S0006-3495(04)74249-6.
1356 Gabbiani F, Dewell R (2018) M-current regulates firing mode and spike reliability in a
1357 collision detecting neuron. bioRxiv:335174 Available at:
1358 https://www.biorxiv.org/content/early/2018/05/31/335174.
1359 Gastrein P, Campanac É, Gasselin C, Cudmore RH, Bialowas A, Carlier E,
1360 Fronzaroli-Molinieres L, Ankri N, Debanne D (2011) The role of
1361 hyperpolarization-activated cationic current in spike-time precision and intrinsic
1362 resonance in cortical neurons in vitro. J Physiol.
1363 Gittelman JX (2006) Kv1.1-Containing Channels Are Critical for Temporal Precision
1364 During Spike Initiation. J Neurophysiol 96:1203–1214 Available at:
1365 http://jn.physiology.org/cgi/doi/10.1152/jn.00092.2005.
1366 Gonçalves JT, Anstey JE, Golshani P, Portera-Cailliau C (2013) Circuit level defects
1367 in the developing neocortex of Fragile X mice. Nat Neurosci.
1368 Gross C, Yao X, Pong DL, Jeromin A, Bassell GJ (2011) Fragile X mental retardation
1369 protein regulates protein expression and mRNA translation of the potassium
1370 channel Kv4.2. J Neurosci 31:5693–5698.
1371 Guan D, Higgs MH, Horton LR, Spain WJ, Foehring RC (2011) Contributions of Kv7-
1372 mediated potassium current to sub- and suprathreshold responses of rat layer
1373 II/III neocortical pyramidal neurons. J Neurophysiol 106:1722–1733 Available at:

http://jn.physiology.org/cgi/doi/10.1152/jn.00211.2011.

Han X, Boyden ES (2007) Multilpe-color optical activation, silencing, and desynchronization of neural activity, with single-spike temporal resolution. PLoS One 2.

Heulens I, D'Hulst C, Van Dam D, De Deyn PP, Kooy RF (2012) Pharmacological treatment of fragile X syndrome with GABAergic drugs in a knockout mouse model. Behav Brain Res.

Hönigsperger C, Marosi M, Murphy R, Storm JF (2015) Dorsoventral differences in Kv7/M-current and its impact on resonance, temporal summation and excitability in rat hippocampal pyramidal cells. J Physiol.

Hou GQ, Pan X, Liao CS, Wang SH, Li DF (2012) SK channels modulate the excitability and firing precision of projection neurons in the robust nucleus of the arcopallium in adult male zebra finches. Neurosci Bull.

Kirischuk S, Voitenko N, Kostyuk P, Verkhratsky A (1996) Age-associated changes of cytoplasmic calcium homeostasis in cerebellar granule neurons in situ: Investigation on thin cerebellar slices. Exp Gerontol.

Kleiman-Weiner M, Beenhakker MP, Segal WA, Huguenard JR (2009) Synergistic Roles of GABA A Receptors and SK Channels in Regulating Thalamocortical Oscillations. J Neurophysiol 102:203–213 Available at: www.jn.org.

Krey JF, Dolmetsch RE (2007) Molecular mechanisms of autism: a possible role for Ca2+ signaling. Curr Opin Neurobiol 17:112–119.

Kwag J, Jang HJ, Kim M, Lee S (2014) M-type potassium conductance controls the emergence of neural phase codes: A combined experimental and neuron modelling study. J R Soc Interface.

Larson J (2005) Age-Dependent and Selective Impairment of Long-Term

1399 Potentiation in the Anterior Piriform Cortex of Mice Lacking the Fragile X Mental
1400 Retardation Protein. J Neurosci.
1401 Laumonnier F, Roger S, Guérin P, Molinari F, M'Rad R, Cahard D, Belhadj A,
1402 Halayem M, Persico AM, Elia M, Romano V, Holbert S, Andres C, Chaabouni H,
1403 Colleaux L, Constant J, Le Guennec JY, Briault S (2006) Association of a
1404 functional deficit of the BKCa channel, a synaptic regulator of neuronal
1405 excitability, with autism and mental retardation. Am J Psychiatry 163:1622–
1406 1629.
1407 Lauterborn JC, Rex CS, Krama E, Chen LY, Pandyarajan V, Lynch G, Gall CM
1408 (2007) Brain-Derived Neurotrophic Factor Rescues Synaptic Plasticity in a
1409 Mouse Model of Fragile X Syndrome. 27:10685–10694.
1410 Lee E, Lee J, Kim E (2017) Excitation/Inhibition Imbalance in Animal Models of
1411 Autism Spectrum Disorders. Biol Psychiatry 81:838–847 Available at:
1412 http://dx.doi.org/10.1016/j.biopsych.2016.05.011.
1413 Lee HY, Ge W-P, Huang W, He Y, Wang GX, Rowson-Baldwin A, Smith SJ, Jan YN,
1414 Jan LY (2011) Bidirectional Regulation of Dendritic Voltage-Gated Potassium
1415 Channels by the Fragile X Mental Retardation Protein. Neuron 72:1091.
1416 Lee HY, Ge W, Huang W, He Y, Wang GX, Smith SJ, Jan YN, Jan LY (2012)
1417 Bidirectional Regulation of Dendritic Voltage-gated Potassium Channels by the
1418 Fragile X Mental Retardation Protein. Neuron 72:630–642.
1419 Limpitikul WB, Dick IE, Ben-Johny M, Yue DT (2016) An autism-associated mutation
1420 in CaV1.3 channels has opposing effects on voltage- and Ca2+ -dependent
1421 regulation. Sci Rep 6:1–13 Available at: http://dx.doi.org/10.1038/srep27235.
1422 Lubs' HA (n.d.) A Marker X Chromosome.
1423 Luque MA, Beltran-matas P, Marin MC, Torres B, Herrero L (2017) Excitability is

1424 increased in hippocampal CA1 pyramidal cells of Fmr1 knockout mice. :1–18.
1425 Madison D V, Lancaster B, Nicoll RA (1987) Voltage Clamp Analysis of Cholinergic
1426 Action in the Hippocampus. 7:733–741.
1427 Markram H, Lu J, Frotscher M, Sakmann B (1997) Regulation of Synaptic Efficacy by
1428 Coincidence of Postsynaptic APs and EPSPs. 275:213–215.
1429 Martin HGS, Lassalle O, Brown JT, Manzoni OJ (2016a) Age-Dependent Long-Term
1430 Potentiation Deficits in the Prefrontal Cortex of the Fmr1 Knockout Mouse Model
1431 of Fragile X Syndrome. Cereb Cortex 26:2084–2092.
1432 Martin HGS, Lassalle O, Brown JT, Manzoni OJ (2016b) Age-Dependent Long-Term
1433 Potentiation Deficits in the Prefrontal Cortex of the Fmr1 Knockout Mouse Model
1434 of Fragile X Syndrome. Cereb Cortex.
1435 Meredith RM, Dawitz J, Kramvis I (2012) Sensitive time-windows for susceptibility in
1436 neurodevelopmental disorders. Trends Neurosci 35:335–344 Available at:
1437 http://dx.doi.org/10.1016/j.tins.2012.03.005.
1438 Meredith RM, Holmgren CD, Weidum M, Burnashev N (2007) Article Increased
1439 Threshold for Spike-Timing-Dependent Plasticity Is Caused by Unreliable
1440 Calcium Signaling in Mice Lacking Fragile X Gene Fmr1. :627–638.
1441 Ngo-Anh TJ, Bloodgood BL, Lin M, Sabatini BL, Maylie J, Adelman JP (2005) SK
1442 channels and NMDA receptors form a Ca2+-mediated feedback loop in dendritic
1443 spines. Nat Neurosci.
1444 Nguyen RL, Medvedeva Y V, Ayyagari TE, Schmunk G, Jay J (2018) BBA -
1445 Molecular Cell Research Intracellular calcium dysregulation in autism spectrum
1446 disorder : An analysis of converging organelle signaling pathways ☆. BBA - Mol
1447 Cell Res 1865:1718–1732 Available at:
1448 https://doi.org/10.1016/j.bbamcr.2018.08.003.

1449 Nigro MJ, Mateos-Aparicio P, Storm JF (2014) Expression and Functional Roles of
1450 Kv7/KCNQ/M-Channels in Rat Medial Entorhinal Cortex Layer II Stellate Cells. J
1451 Neurosci 34:6807–6812 Available at:
1452 http://www.jneurosci.org/cgi/doi/10.1523/JNEUROSCI.4153-13.2014.
1453 Nimchinsky E a, Oberlander a M, Svoboda K (2001) Abnormal development of
1454 dendritic spines in FMR1 knock-out mice. J Neurosci 21:5139–5146.
1455 O'Donnell WT, Warren ST (2002) A Decade of Molecular Studies of Fragile X
1456 Syndrome. Annu Rev Neurosci.
1457 Orban G, Kiss T, Erdi P (2006) Intrinsic and Synaptic Mechanisms Determining the
1458 Timing of Neuron Population Activity During Hippocampal Theta Oscillation. J
1459 Neurophysiol 96:2889–2904 Available at:
1460 http://jn.physiology.org/cgi/doi/10.1152/jn.01233.2005.
1461 Paradee W, Melikian HE, Rasmussen DL, Kenneson A, Conn PJ (1999) FRAGILE X
1462 MOUSE : STRAIN EFFECTS OF KNOCKOUT PHENOTYPE AND EVIDENCE
1463 SUGGESTING DEFICIENT AMYGDALA FUNCTION. 94:185–192.
1464 Pfeuty B, Mato G, Golomb D, Hansel D (2003) Electrical synapses and synchrony:
1465 the role of intrinsic currents. J Neurosci 23:6280–6294 Available at:
1466 http://www.ncbi.nlm.nih.gov/pubmed/12867513.
1467 Pinggera A, Lieb A, Benedetti B, Lampert M, Monteleone S, Liedl KR, Tuluc P,
1468 Striessnig J (2015) Archival Report CACNA1D De Novo Mutations in Autism
1469 Calcium Channels. Biol Psychiatry 77:816–822 Available at:
1470 http://dx.doi.org/10.1016/j.biopsych.2014.11.020.
1471 Place W (2016) disorders. 77:1079–1088.
1472 Radwan B, Dvorak D, Fenton AA (2016a) Impaired cognitive discrimination and
1473 discoordination of coupled theta-gamma oscillations in Fmr1 knockout mice.

1474 Neurobiol Dis 88:125–138 Available at:
1475 http://dx.doi.org/10.1016/j.nbd.2016.01.003.
1476 Radwan B, Dvorak D, Fenton AA (2016b) Impaired cognitive discrimination and
1477 discoordination of coupled theta-gamma oscillations in Fmr1 knockout mice.
1478 Neurobiol Dis.
1479 Routh BN, Johnston D, Brager DH (2013) Loss of functional A-type potassium
1480 channels in the dendrites of CA1 pyramidal neurons from a mouse model of
1481 fragile X syndrome. J Neurosci 33:19442–19450 Available at:
1482 http://www.ncbi.nlm.nih.gov/pubmed/24336711.
1483 Sah P, Clements JD (1999) Photolytic Manipulation of [Ca 2 ⁄] i Reveals Slow
1484 Kinetics of Potassium Channels Underlying the Afterhyperpolarization in
1485 Hipppocampal Pyramidal Neurons. 19:3657–3664.
1486 Schultheiss NW, Edgerton JR, Jaeger D (2010) Phase Response Curve Analysis of
1487 a Full Morphological Globus Pallidus Neuron Model Reveals Distinct
1488 Perisomatic and Dendritic Modes of Synaptic Integration. J Neurosci.
1489 Sourdet V, Russier M, Daoudal G, Ankri N, Debanne D (2003) Long-Term
1490 Enhancement of Neuronal Excitability and Temporal Fidelity Mediated by
1491 Metabotropic Glutamate Receptor Subtype 5.
1492 Stevens CF, Zador a M (1998) Input synchrony and the irregular firing of cortical
1493 neurons. Nat Neurosci 1:210–217 Available at:
1494 http://www.ncbi.nlm.nih.gov/pubmed/10195145.
1495 Strumbos JG, Brown MR, Kronengold J, Polley DB, Kaczmarek LK (2010) Fragile X
1496 Mental Retardation Protein Is Required for Rapid Experience-Dependent
1497 Regulation of the Potassium Channel Kv3 . 1b. 30:10263–10271.
1498 Talbot ZN, Sparks FT, Dvorak D, Curran BM, Alarcon JM, Fenton AA (2018a)

1499 Normal CA1 Place Fields but Discoordinated Network Discharge in a Fmr1-Null
1500 Mouse Model of Fragile X Syndrome. Neuron:684–697.
1501 Talbot ZN, Sparks FT, Dvorak D, Curran BM, Alarcon JM, Fenton AA (2018b)
1502 Normal CA1 Place Fields but Discoordinated Network Discharge in a Fmr1-Null
1503 Mouse Model of Fragile X Syndrome. Neuron.
1504 Tang B, Wang T, Wan H, Han L, Qin X, Zhang Y, Wang J, Yu C, Berton F,
1505 Francesconi W, Yates JR, Vanderklish PW, Liao L (2015) *Fmr1* deficiency
1506 promotes age-dependent alterations in the cortical synaptic proteome. Proc Natl
1507 Acad Sci 112:E4697–E4706 Available at:
1508 http://www.pnas.org/lookup/doi/10.1073/pnas.1502258112.
1509 Tessier CR, Broadie K (2011) Neurobiology of Disease The fragile X mental
1510 retardation protein developmentally regulates the strength and fi delity of
1511 calcium signaling in Drosophila mushroom body neurons. Neurobiol Dis 41:147–
1512 159 Available at: http://dx.doi.org/10.1016/j.nbd.2010.09.002.
1513 Testa-Silva G, Loebel A, Giugliano M, De Kock CPJ, Mansvelder HD, Meredith RM
1514 (2012) Hyperconnectivity and slow synapses during early development of
1515 medial prefrontal cortex in a mouse model for mental retardation and Autism.
1516 Cereb Cortex 22:1333–1342.
1517 Tian Y, Yang C, Shang S, Cai Y, Deng X, Zhang J, Shao F, Zhu D, Liu Y, Chen G,
1518 Liang J, Sun Q, Qiu Z, Zhang C (2017) Loss of FMRP Impaired Hippocampal
1519 Long-Term Plasticity and Spatial Learning in Rats. Front Mol Neurosci 10:1–14
1520 Available at: http://journal.frontiersin.org/article/10.3389/fnmol.2017.00269/full.
1521 Zhang Y, Bonnan A, Bony G, Ferezou I, Pietropaolo S, Ginger M, Sans N, Rossier J,
1522 Oostra B, LeMasson G, Frick A (2014) Dendritic channelopathies contribute to
1523 neocortical and sensory hyperexcitability in Fmr1−/y mice. Nat Neurosci

1524 17:1701–1709 Available at:
1525 http://www.nature.com/doifinder/10.1038/nn.3864%5Cnhttp://dx.doi.org/10.1038
1526 /nn.3864.
1527 Zhu P, Li J, Zhang L, Liang Z, Tang B, Liao WP, Yi YH, Su T (2018) Development-
1528 related aberrations in Kv1.1 α-subunit exert disruptive effects on bioelectrical
1529 activities of neurons in a mouse model of fragile X syndrome. Prog Neuro-
1530 Psychopharmacology Biol Psychiatry 84:140–151 Available at:
1531 https://doi.org/10.1016/j.pnpbp.2018.02.011.
1532
1533
1534